UiT
THE ARCTIC
UNIVERSITY
OF NORWAY

Department of Physics and Technology

Super-Resolution Imaging of Sub-Mitochondrial Structures using Structured Illumination Microscopy

—

Ida Sundvor Opstad

FYS-3900 Master's Thesis in Physics
May 2016

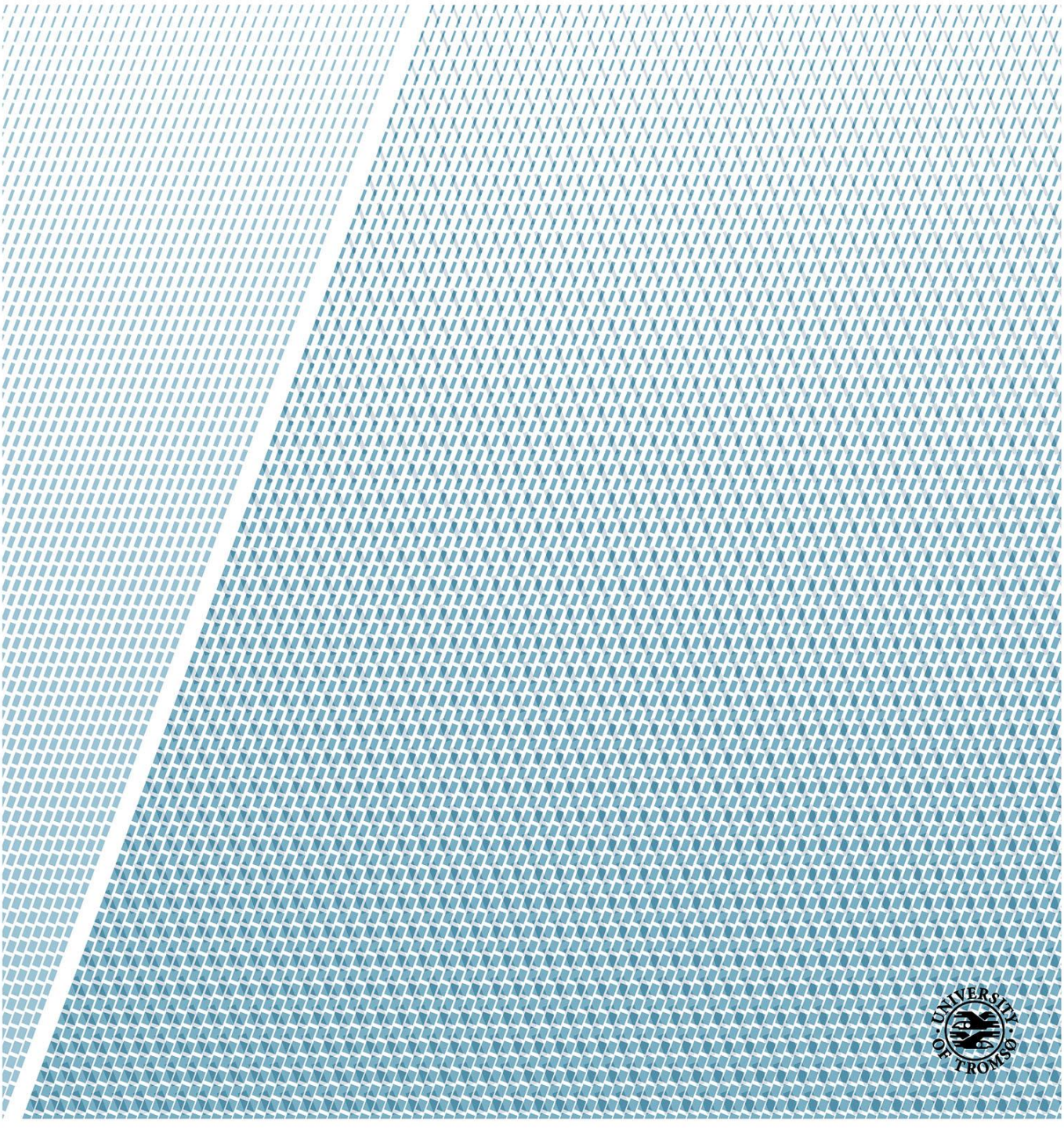

Abstract

Modern science is based on observation, and its advances are limited by what is possible to observe. For centuries optical microscopy was limited by the diffraction of light, making structures closer together than half the wavelength of light unresolvable. In recent years, the new field of optical nanoscopy has emerged, enabling diffraction-limited structures to be resolved. As opposed to electron microscopy, optical microscopy enables observing biological samples *live*. The new observational tools give hope for a revolution within biological sciences, because a much closer look at inter- and intracellular processes has become possible. Observing is, however, not without affecting the system under observation. This becomes especially evident while observing living nano-structures.

Here, I optimize parameters for live cell imaging by structured illumination microscopy (SIM) and compare the results with diffraction-limited microscopy. Specifically, I target different mitochondrial structures by combining both dual transfection with MitoTracker labeling, which results in the ability to resolve three different mitochondrial structures at once in living cells.

Time-lapse imaging was done with SIM and also compared with diffraction-limited deconvolution microscopy (DV). SIM required higher signal-to-noise ratios for successful imaging and was light intensive compared to DV. SIM caused quick photobleaching of the sample (limiting the number of frames possible) and clear phototoxic effects, resulting in morphological artifacts. In comparison, time-lapse with DV enabled more time points, larger field of view and eliminated any apparent morphological artifacts. Mitochondrial and (diffraction-limited) fenestration *dynamics* in the membrane of liver sinusoidal endothelial cells was also captured using SIM, and, finally, SIM artifacts and challenges are discussed.

While optical nanoscopy could still be a preferred option for imaging a few time-points of diffraction-limited structures, the extra photon cost still makes DV a better tool for studies not strictly requiring the higher resolution (like monitoring mitochondrial dynamics). This points future development of live cell nanoscopy in the direction of lower illumination intensities coupled with (non-toxic) brighter and photostable fluorophores. The preferred imaging tool would be an optical platform allowing for specific application-tailored resolution, minimizing the phototoxicity and photobleaching with a flexible field of view.

Introduction and Purpose

The *resolution limit* describes a minimal distance between adjacent structures that can be resolved by a perfect conventional optical microscope. While optical microscopes have for a long time been used to study individual cells and larger sub-cellular structures, the about 200 nm resolution limit has restricted the study of smaller structures, especially within living cells.

In recent years, ways around this limit have been found and have given birth to the new science of *optical nanoscopy*. It is also often called *super-resolution microscopy*, and enables imaging at *super-resolution* (SR), meaning the ability to distinguish between two structures closer together than approximately 200 nm.

An optical microscope enabling super-resolution with structured illumination microscopy (SIM) (commonly referred to as the OMX) was installed at the technology building at the same time as I started my master's project in Physics. I became the first student to be trained on this nanoscope, and during my master's project, I became an independent user of this complex optical instrument both concerning the data acquisition and reconstruction, followed by analysis (in Fiji and Volocity). While completing this thesis I have probably spent more hours than anyone else on this state-of-the-art nanoscope.

In contrast with (for example) electron microscopy, SIM enables SR of *living* samples, extending the limits of what is possible to study within the life sciences. To become a fully independent user of this new live cell imaging tool, I was also trained in biology, cell culture and staining in close collaboration with Vascular Biology Research Group (VBRG) at the Department of Medical Biology.

SR imaging, especially of living samples, is not straight forward and many parameters must be optimized to make the new nanoscope a useful research tool. This master's project has been about optimization of parameters for live cell nanoscopy with SIM. The main focus has been on multicolor labeling of mitochondria in cell lines, but also of the cell membrane (and mitochondria) of liver sinusoidal endothelial cells (LSECs).

Since the discovery of optical nanoscopy techniques, extensive work has been done on imaging mitochondria but this has been mostly limited to fixed cells[24][38]. There are only a few reported papers on imaging mitochondrial dynamics in living cells using optical nanoscopy[16][39], though a thorough literature review is beyond the scope of this thesis. However, to the best of our knowledge, there is very little work done on multicolor imaging of sub-

mitochondrial regions in living cells using optical nanoscopy.

My work during this master's project has resulted into four conference posters, with one of these having me (Ida S. Opstad) as the first author. In addition, the manuscript for a peer-reviewed journal is being prepared, also with me as the first author.

In some experimental periods, I did it all: planning, cell culture, staining, imaging and image processing. For other experiments, cells were already plated and/or stained for me. This cell work was done mostly by Cristina[1], but also Deanna[2], Hong[3] and Cristiane[4]. Elizabeth[5] was indispensable in the culturing of gene modified (GM) bacteria and in obtaining pDNA for transfection experiments. The GM bacteria were bought from Addgene (plasmids numbers 54282 and 55328), and the particular plasmids used were donated to Addgene by Michael W. Davidson.

The following chapter contains theoretical background for understanding fluorescence nanoscopy and the results discussed in Chapter 3. Chapter 2 gives detailed experimental descriptions, and Chapter 4 the conclusions. Chapter 5 contains the list of publications.

[1] Cristina I. Øie, Department of Physics and Technology (previously Department of Medical Biology)

[2] Deanna L. Wolfson, Department of Physics and Technology

[3] Hong Mao, Department of Medical Biology

[4] Cristiane de A. C. Jacobsen, Department of Pharmacy

[5] Elizabeth G. A. Fredheim, Department of Microbiology

Acknowledgments

I would like to thank all my collaborators for being uttermost welcoming, helpful and providing me access to places physicists should never be allowed. My greatest thanks goes to my supervisors, B&D, for exquisite guidance and for making it all possible.

Contents

List of Figures

Abbreviations

BM CellLight Mitochondrial RFP BacMam 2.0

CMdr CellMask Deep Red

CMO CellMask Orange

FP fluorescent protein

Gtom GFP targeting TOM20

MOM mitochondrial outer membrane

MT MitoTracker

MTdr MitoTracker Deep Red

MTG MitoTracker Green

PFA paraformaldehyde

SIM Structured illumination microscopy

SMLM Single molecule localazation microscopy

STED Stimulated emission depletion microscopy

TOM20 translocase of outer membrane 20 kDa subunit

Nomenclature

R_A Abbe limit

OMX nanoscope enabling SIM at UiT

s/n signal-to-noise ratio

Chapter 1

Fluorescence Nanoscopy

This chapter contains relevant theory for understanding the basics of fluorescence nanoscopy.

1.1 Optical Microscopy

1.1.1 The Wave Model of Light: *Limitations of Optical Microscopy*

Optical microscopy enables seeing structures smaller than what is possible with our eyes alone by utilizing light and optical components. The optical components are primarily lenses put together to form a microscope, enabling a magnified image of an object of interest.

The optical microscope was optimized over centuries to enable the study of smaller and smaller structures. Ultimately, this led to the discovery of *the diffraction* (or *resolution*) *limit*, which is the best resolution obtainable with a (perfect) conventional optical microscope.

The resolution limit can be explained using the *wave model* of light. Like e.g. water waves when interacting with matter, light diffracts and interferes with itself. The resulting intensity patterns can be found as solutions to wave equations. Still, when using light for seeing structures smaller than about half the wave length of light (with a perfect conventional microscope), a fundamental problem is soon encountered.

An emitting point object in the microscope, like a fluorescent molecule (or *fluorophore*), will produce an image that consists of a diffraction pattern known as an *Airy pattern*. In three-dimensions (3D), this intensity distribution is referred to as the point spread function (PSF). To illustrate how this limits resolution, consider Figure 1.1, where two adjacent Airy patterns are shown at varying distances apart. The question of resolution is now more obvious: *How close can two emitting points be before we no longer can tell them apart*?

The central spot of an Airy pattern is called an *Airy disc*, and several math-

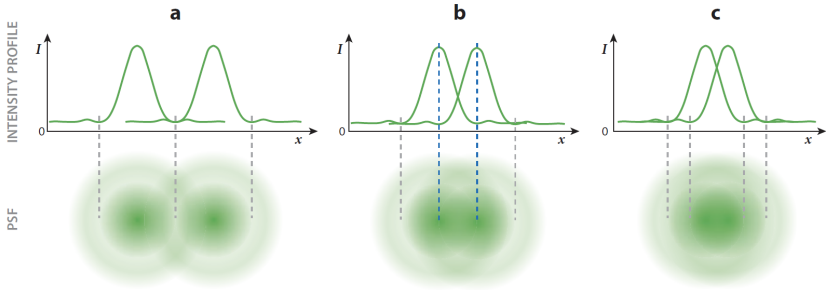

Figure 1.1: (*Bottom*) Point spread functions modeled as Airy discs of two neighboring emitting points. (*Top*) The corresponding intensity profiles. (**a**) Resolved emitters, (**b**) separation *at* the Rayleigh resolution limit R_R, (**c**) unresolved emitters.[4]

ematical definitions of resolution have been based on this very spot. The size of the Airy disc is related to the wavelength of light (λ) and the numerical aperture (NA) of the objective, which is a measure of the light gathering abilities and (therefore) the resolution of the objective.

Ernst Karl Abbe (in 1873) defined the resolution as *the radius of the Airy disc*,

$$R_A = \frac{\lambda}{2\,NA} \tag{1.1}$$

while Lord Rayleigh (in 1896) defined the resolution limit as the distance between two emitters when the central spot (or maximum) of the Airy disk from one overlaps with the first minimum of the second (see figure 1.1**b**),

$$R_R = \frac{1.22\,\lambda}{2\,NA}. \tag{1.2}$$

By definition, $R_A = 1.22R_R$, so if two points are farther apart than R_R (rarely less than 200nm), you should be able to see them as separate (in a perfect optical microscope), but not of they are closer than R_A. 'Able to tell two emitters apart' is somewhat subjective, thus we have multiple definitions.[2][3][4][11]

1.1.2 The Particle Model of Light: *Fluorescence Microscopy*

Quanta of light energy are called *photons*, and *the Planck-Einstein relation* gives the connection between the photon energy (E), frequency (f), speed (c) and wavelength (λ),

$$E = hf = hc/\lambda \tag{1.3}$$

Photons can be absorbed and reemitted by a substance, usually at a longer wavelength (and lower energy). This physical phenomenon is known as *fluorescence*,

and is often illustrated through a *Jablonski diagram*, as shown in Figure 1.2. The horizontal lines indicate electronic energy states of a fluorescent molecule (called a *fluorophore*), with the thin lines being vibrational/rotational sublevels of the electronic energy levels indicated by bold (horizontal) lines. Atoms are (at earth) most of the time in *the ground state* S_0, where they are *non*-excited. The numbers indicate typical timescales for the transition events.[1][19]

The probability that a photon will be absorbed varies with many things, including the wavelength. Each fluorophore has its own characteristic excitation and emission spectrum, providing a statistical description of how the fluorophore responds when subjected to radiation.[7]

Figure 1.3 shows a typical absorption and emission spectrum. The excitation maximum, 532 nm in this case, is the wavelength most likely to excite this dye, and the emission maximum, 557 nm, is the wavelength most likely to be re-emitted. The difference between the excitation and emission maximum is called the Stokes' shift, and is in this example 25 nm.

In fluorescence microscopy, fluorophores are extensively used to label samples for increased contrast. This way one can gain knowledge about *what* the different structures are, and not just 'how far they are apart'. This is done, for example, by attaching the fluorophore to a molecule which is known to bind to the structure one wishes to investigate. Some materials are intrinsically fluorescent (autofluorescent), while others are fluorescent only upon binding to specific structures.

To clearly separate the light shone *on* the sample from the light emitted *by* the sample, chromatic filters are used. Here a large Stokes' shift is preferable. To (e.g.) image something labeled with the dye Rhodamine 6G, one would optimally use an excitation laser with wavelength 532 nm and a chromatic filter with bandpass 540-570 nm to separate scattered light from light emitted by the dye. The availability of lasers and dyes with different spectra, gives the opportunity for multicolor imaging.

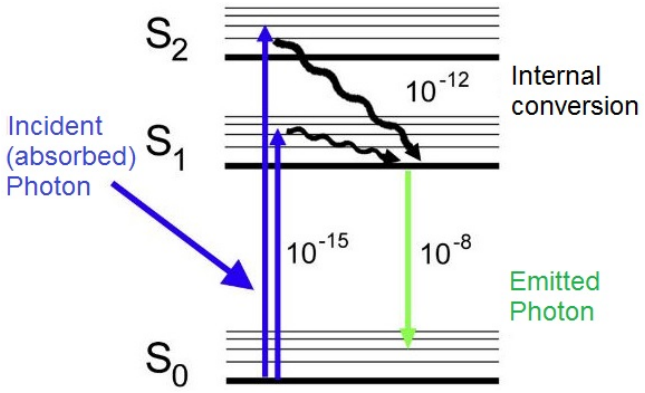

Figure 1.2: *Jablonski diagram* indicating electronic states (thick lines) and vibrational states (thin lines) of a fluorescent molecule and typical timescales (in seconds) for the transition events involved in fluorescence.[20]

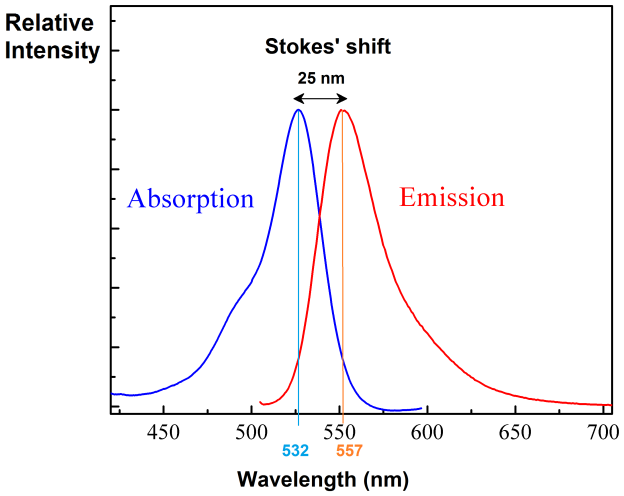

Figure 1.3: *Absorption and emission spectrum* of the dye Rhodamine 6G. Absorption maximum: 532 nm, emission maximum: 557 nm, and 25 nm Stokes' shift.[21]

1.2 Beyond the Diffraction Limit: *Nanoscopy Techniques*

Super-resolution can be accomplished by different techniques. The current three main methods for fluorescence nanoscopy can be divided into SIM, STED and SMLM. An overview of these is given in this section.

1.2.1 Single-Molecule Localization Microscopy

Single molecule localization microscopy (SMLM) consists of several techniques such as dSTORM (direct stochastic optical reconstruction microscopy), PALM (photo activation localization microscopy) and others. SMLM separates the information in *time* instead of space. The working principle of SMLM can be explained through Figure 1.4: **a** shows a sample consisting of many point sources (fluorophores) together forming or labeling a net (of e.g. a filamentous cell protein). **b** shows how these point emitters (together) would look like in a conventional fluorescence microscope, and **c** how this same net of emitters would look like when only *a few* separated molecules are emitting light at the same time. Even though image **c** is still diffraction-limited, the position of the emitters can be determined more precisely (with higher resolution) by doing a 2D-Gaussian fit, resulting in image **d**. Saving this image (of a small sub-set of emitters) and making sure the fluorophores are blinking (switching between dark and emitting states), a different sub-set of fluorophores can be imaged after a (preferably short) time-interval, as shown in **e**. **f** shows the resulting (super-resolved) image after many frames and single-molecule localizations have been added together.

There is no 'fundamental limit' to how precisely you can determine the location of fluorophores in this manner, but the practical resolution is limited by labeling density, label size, bleaching, noise and how long you are willing to capture 'single-photon frames'. The biggest drawbacks are long acquisition times (for high resolution) and the requirement of suitable blinking/photoswitchable fluorophores, dependent on the specific SMLM technique used.[3][4][5]

1.2.2 Stimulated Emission Depletion Microscopy

Stimulated emission depletion microscopy (STED) works by reducing the size of the region in the sample capable of spontaneously emitting light. When the excitation light is sent through an objective and focused on a sample it will be no smaller than the PSF of the focusing objective. To make the region containing excited molecules smaller, a doughnut-shaped laser beam at a longer wavelength is placed surrounding the exciting beam, depleting (or 'emptying') the doughnut shaped region of excited molecules through stimulated emission. The stimulated emitting atoms will emit photons at a wavelength and phase identical to that of the (longer wavelength) depleting laser, and at a shorter time scale compared to the spontaneously emitted photons (from the middle of the doughnut). The photons from the center of the doughnut can therefore

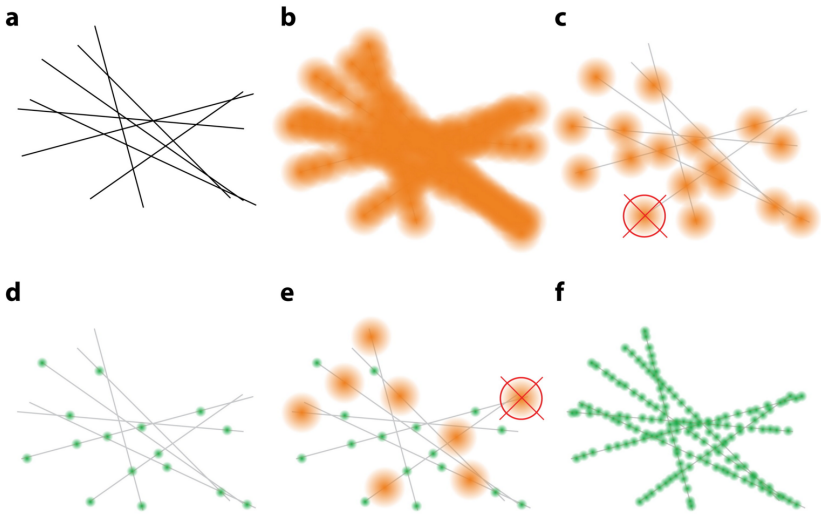

Figure 1.4: *Working principles of single-molecule localization microscopy (SMLM).* **a**: Sample consisting of many point sources (fluorophores) together forming/labeling a net. **b**: Conventional fluorescence microscope image of all fluorophores emitting together. **c**: Same sample (and microscope) when only *a few* separated molecules are emitting light at the same time. **d**: 2D-Gaussian fit resulting in more precise localization of emitting fluorophores. **e**: Blinking of the fluorophores (switching between dark and emitting states) allows for a different sub-set of fluorophores to be imaged (and statistically more precisely localized) at a later time. **f**: Resulting super-resolved image after many frames and single-molecule localizations have been added together.[4]

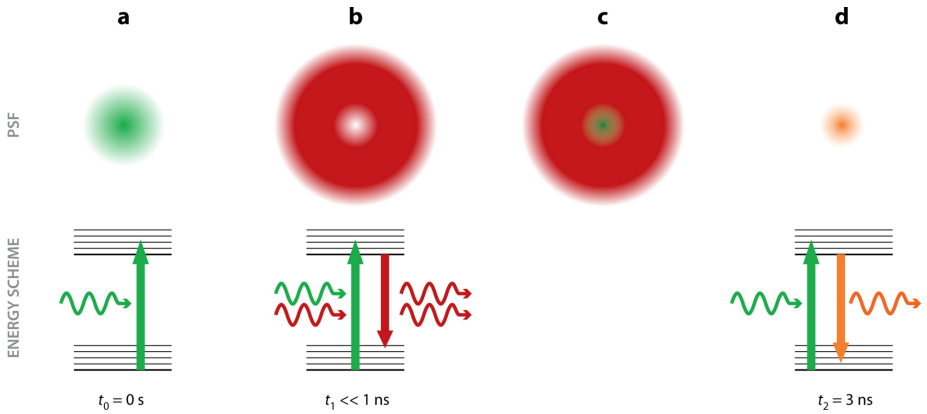

Figure 1.5: Principles of STED. *Top*: **a**: Excitation point spread function (PSF). **b**: Shape of longer λ depleting laser beam. **c**: Superimposed beams. **d**: Reduced excitation spot. *Bottom*: Corresponding energy transitions and timescales for **a**, **b** and **d**.[4]

be separated (e.g. by using a chromatic filer) from the peripheral photons, and super-resolved information obtained. This is illustrated in Figure 1.5. The entire region of interest is scanned by the combined laser beam and a super-resolved image obtained, pixel-by-pixel.

Drawbacks include high input of laser energy (unsuited for live cell imaging), long scanning times (for larger regions) and the requirement of fluorophores with energy states that fit the available laser set up.[3][4]

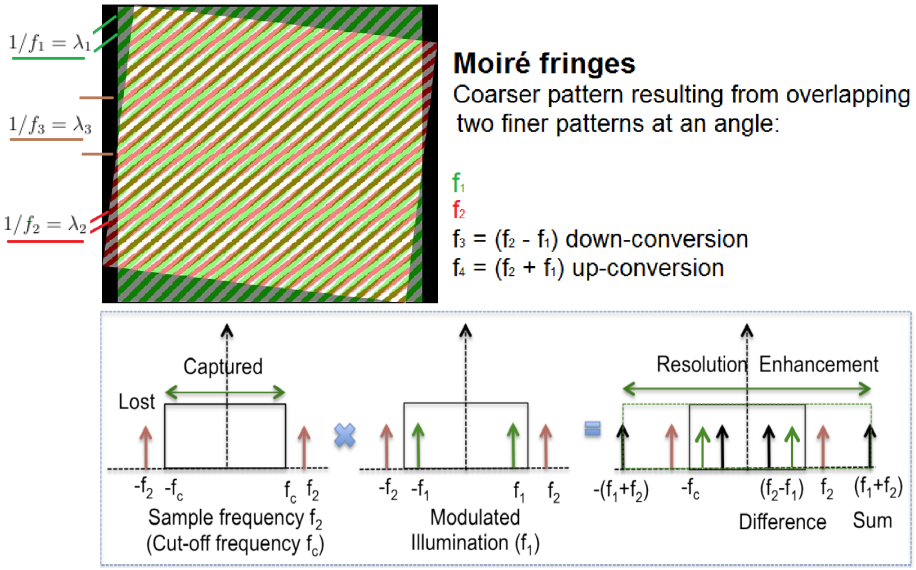

Figure 1.6: Principles of SIM. Overlapping two striped patterns of frequencies f_1 and f_2 leads to additional components at higher $(f_1 + f_2)$ and lower $(f_2 - f_1)$ frequencies. The coarser pattern is known as Moiré fringes. f_c represents the cut-off frequency of the microscope objective. With structured illumination microscopy, one can calculate higher frequencies $(f_3 = f_1 + f_2)$ and obtain super-resolved information.

1.2.3 Structured Illumination Microscopy

The resolution limit (R) of a conventional microscope was introduced in section 1.1.1 in the spatial domain. From the frequency domain perspective, this limit is the inverse (1/R) and this defines the *cut-off frequency* (f_c) for the microscope. The point-spread function (PSF) becomes an *optical transfer function* (OTF), defined as the Fourier transform of the microscope's PSF.

The limited resolution of a conventional microscope can be explained by the loss of high frequency information, so that the objective can be modeled as a low pass filter (removing frequencies above f_c). Structured illumination microscopy (SIM) recovers information *above* f_c through computational post-processing after illuminating the sample with a striped pattern of light created by interference, which is resolvable below f_c.

This can be visualized by overlapping two fine patterns at an angle, and noticing the coarser (lower f) pattern appearing, as shown in Figure 1.6 (*top*). The resulting coarser pattern is called *Moiré fringes*. The lower part of the same figure illustrates how frequency mixing results in resolution enhancement. f_1 is the (known) structured illumination, f_2 is the (unknown) sample structure, and

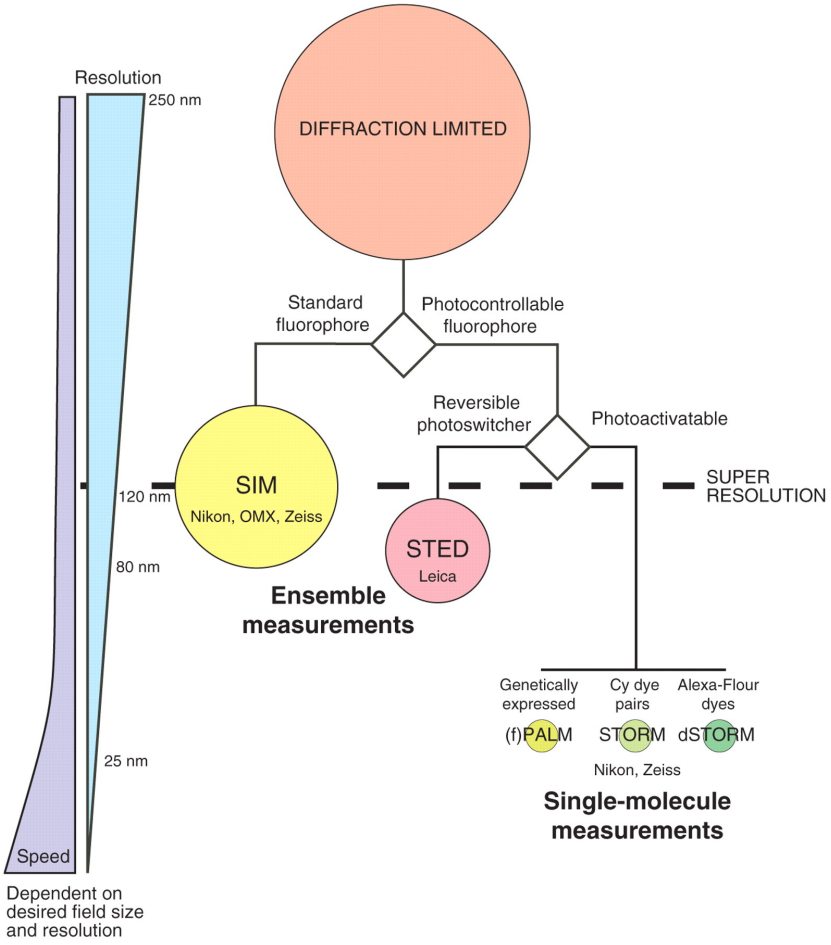

Figure 1.7: *Overview of fluorescence microscopy techniques.* SIM is the fastest super-resolution technique, but offers only a two-fold resolution enhancement compared to diffraction-limited microscopy. STED offers higher resolution but is a slower (point-scanning) technique. PALM, fPALM, STORM and dSTORM are sub-techniques of SMLM and offer the highest available resolution, but at a high cost of speed and sample preparation.[3]

$f_3 = f_2 - f_1$ is measured for finding $|f_2| = |f_1| + |f_3|$ (fine sample details). Since $f_3 = f_2 - f_1 \leq |f_c|$ and $|f_1| \leq |f_c|$, we get $|f_2| \leq |2f_c|$, meaning a maximum resolution enhancement of 2X, in practice about 100 nm.[3][4][14]

A typical choice for the structure of the illumination pattern is sinusoidal stripes illuminating the sample sequentially from different angles and with different phase shifts. For example, the 3D-SIM technique of the OMX illuminates the sample 15 times for each 2D plane, including five phase shifts at three different angles, and repeats this in 8 different focal (z-) planes for each µm of thickness. This means acquiring $5 \times 3 \times 8 = 120$ images per one micron thick stack. The total acquisition time depends on choice of exposure time, but typically is one to five seconds.

Choosing the Right Technique

Choosing the right technique for one's imaging application is crucial. Knowing the approximate size and time scale for the events one wants to capture is essential, both in the planning and imaging phase. This is because higher resolution is (in general) at the cost of speed, as illustrated in Figure 1.7. Conventional (diffraction-limited) microscopy is at the top in the figure, providing the lowest resolution but often the highest speed. For imaging applications not requiring more than 200 nm resolution (which is already quite good), conventional microscopy typically is the best.

Going below the diffraction limit, SIM is currently the best option for live cell imaging applications, even though other techniques can obtain higher resolution. This is because of the higher imaging speed and typically far gentler illumination intensities, e.g. $10^3 - 10^8 W/cm^2$ *lower* than for STED, which is less damaging to living cells. Since SIM also works with many conventional fluorescent stains, multi-color imaging is relatively easy. When SIM does not provide sufficient resolution for one's imaging application (requires better than about 100 nm), one should consider STED and/or SMLM. [3][23]

1.3 Preparing Biological Samples for Fluorescence Microscopy

Fluorescence nanoscopy has the strict requirement of fluorescently-labeled structures. This section describes different pathways for introducing fluorophores onto biological structures, and extra considerations concerning live cell imaging.

1.3.1 Fixation and Immunolabeling

Fixation is done to preserve the shape of living cells (after death), since they rapidly disassemble when untreated. Fixation can be done in many ways, but the most common for fluorescence microscopy is chemically using formaldehyde

(CH_2O) derived from paraformaldehyde (PFA) or formalin (since formaldehyde is a gas at room temperature). It preserves the cellular structures by cross-linking proteins via methylene bridges ($-CH_2-$), eventually fixing/preserving the cell shape.

Fixation allows for more flexibility when it comes to both imaging and labeling. Variables like imaging environment and time of acquisition are much less strict than when performing live cell imaging. Another huge advantage is the possibility for subsequent *immunolabeling* with *antibodies*.

Immunolabeling is an extensively used method for labeling of proteins in fixed cells. The labels are called *antibodies*, and the molecules they bind to *antigens*. Antibodies are produced by inducing an immune response in animals. A specific fluorescent label is made by covalently linking the antibody to a fluorophore with desirable photophysical properties.

The large size ($\approx$ 10 nm) of antibodies makes them unsuited for live cell imaging of anything not on the outer membrane, since extensive *permeabilization* (dissolving the cell membrane) is required for the antibodies to reach the relevant antigens inside the cell.[27][28]

Alternatives for live cell labeling are described in the next section.

1.3.2 Probing Live Cells

Imaging Environment

Having living cells on the microscope requires some extra considerations. Both for morphological and functional studies, the imaging should take place in an environment favorable for the specific cells under investigation. This is because small changes in the sample environment can have significant effects on both cell function and morphology. As for ordinary cell culture, variables to consider include humidity, temperature, gases, osmolarity, pH, nutrients, etc. Additional requirements for nanoscopy includes minimizing damage from staining and light.[12]

Phototoxicity and Photobleaching

Phototoxicity and photobleaching are among the most limiting factors in 4D nanoscopy (3D + time). Photobleaching is permanent fading of the fluorophores (leaving previously-labeled structures invisible), while phototoxicity refers to *damaging chemical species* resulting from laser illumination of (labeled or unlabeled) cells, most notably reactive oxygen species (ROS). ROS can react with proteins and DNA, causing cell damage, or with fluorophores, causing photobleaching.[46]

To reduce these unwanted effects, one should keep the illumination and fluorophore density minimal. This gives a lower signal-to-noise ratio (s/n), which can easily degrade the image quality. What is a sufficient quality will depend on the imaging application.

Besides reducing light intensities and fluorophore density, some labels are less toxic to cells, and hence more suitable for live cell imaging. One class of

such markers are fluorescent proteins (FPs).[8][17] A common way of introducing FPs into cells is described in the next section.

Transfection

Transfection is a method for transferring foreign DNA into cultured cells. This technique was explored in this project to enable specific labeling for live cell fluorescence nanoscopy of different mitochondrial structures. The DNA was acquired utilizing gene modified (GM) bacteria to produce *plasmids* containing the needed DNA.

Plasmids are small pieces of (extra-chromosomal) DNA, which some bacteria are able to produce considerable amounts of. This makes bacteria experts in *horizontal gene transfer*, meaning that they quickly can share DNA with an entire culture, instead of only to their offspring. For example, a useful plasmid for bacteria can be one with genes for antibiotics resistance[31], while a useful plasmid for a master's student can be one that makes mitochondria fluorescent.

When the DNA transfer is virus-mediated, the word *transduction* is often used instead. This is the function of the commercially available BacMam reagents. They are ready and easy to use, while plasmid DNA (pDNA) from bacteria typically needs to be grown and purified.[34][36]

A drawback of transfection as a form of labeling is that the protein morphology and functions are not necessarily the same in transfected cells as in the cells one originally wanted to study. By contrast, the protein itself is now bigger, including additional FPs of considerable size (e.g. GFP consists of 238 amino acids[32]). The expression level of FPs is also prone to vary by several orders of magnitude, excluding this method from many quantitative studies[29].

Probing Mitochondria

Humans (like other animals) are made of *eukaryotic cells*, and on average, each human has about $3.72 \cdot 10^{13}$ ($= 37\,200\,000\,000\,000$) of them[33]. They are quite small, but not smaller than what is possible to study using a conventional light microscope. With an average volume estimated to be $4 \cdot 10^{-9}\, cm^3$ [33], and assuming a spherical shape, this gives a cell diameter of about 20 µm, 100 times bigger than the diffraction limit ($R \approx 0.2$ µm). The *organelles*, or *internal components*, of eukaryotic cells have been extensively studied using fluorescence microscopy. It has allowed for mapping of many organelles, as shown in Figure 1.8. One of these organelles is *mitochondria*: essential organelles responsible for the availability of ATP (easily accessible chemical energy) generated by 'burning sugar'[41].

The internal structures of mitochondria are beyond the diffraction limit and were only resolvable using electron microscopy before the advent of optical nanoscopy. The scope of this thesis was to optimize staining and imaging parameters for live-cell imaging using SIM to enable visualization of different mitochondrial regions, individually and together. This mapping of mitochondrial

internal structures was done by using selectivity of fluorescent probes coupled with different excitation/emission spectra.

Two main types of probes for mitochondria were explored: MitoTracker (MT) and fluorescent proteins (FPs). The MitoTracker probes (commercially available from Thermo Fisher Scientific) are positively charged ions that accumulate in mitochondria due to the negative transmembrane potential ($\Delta\Psi$) of active mitochondria.[39] MT is available in several colors, and is thought to diffuse across the mitochondrial outer membrane (MOM), but not through the mitochondrial inner membrane (MIM).

The FPs were genetically encoded into cell lines using two different methods: BacMam transduction, and transfection via lipofectamine with plasmid DNA (pDNA) purified from genetically modified bacteria (as discussed in the previous section). The BacMam reagents are commercially available and ready to use. Specifically, *CellLight Mitochondria-RFP, BacMam 2.0* (BM) was used. This reagent labels the enzyme *E1 alpha pyruvate dehydrogenase* in the mitochondrial matrix with red FP (RFP)[36]. The pDNA used labels the mitochondrial outer membrane (MOM) protein TOM20 with green or blue FP (from two different plasmids grown separately).

Figure 1.9 shows a sketch of a mitochondrion with one of the tested staining configurations. The outer membrane protein TOM20 is labeled with GFP (Gtom) with excitation wavelength (ex. λ) 488 nm (turquoise), the intermembrane space is labeled using MitoTracker deep red (MTdr) with ex. λ=642 nm (red), and the mitochondrial matrix is labeled using BM with ex. λ=568 nm (green). Using this scheme, each part of the mitochondrion can be individually identified due to the spectral separation of the fluorophores.

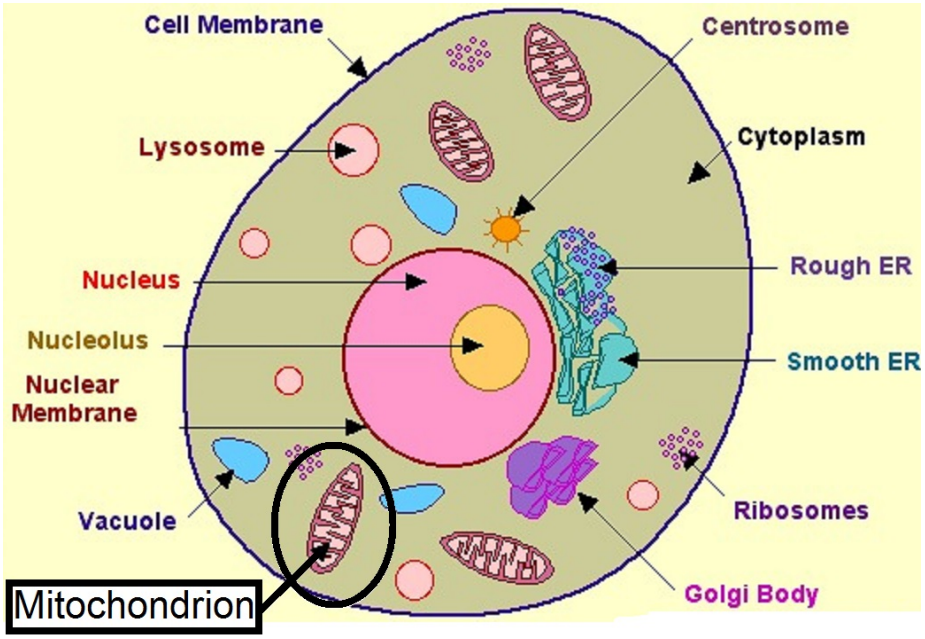

Figure 1.8: Eukaryotic animal-cell with different organelles indicated by arrows. A mitochondrion is highlighted/circled in the lower left.[22]

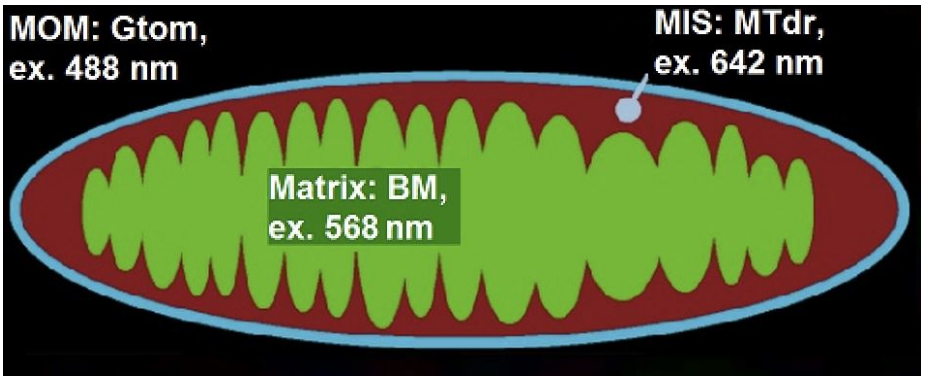

Figure 1.9: *Sketch of mitochondrial structures with live cell probes.* Specificity of probes coupled with different fluorescent excitation/emission spectra and *nanoscopy* allows for mapping of the internal structures of mitochondria: mitochondrial outer membrane (MOM) is labeled with Gtom (ex. λ=488 nm) (turquoise), mitochondrial intermembrane space (MIS) with MitoTracker Deep Red (ex. λ=642 nm) (red), and the mitochondrial matrix is labeled using BM (ex. λ=568 nm) (green).

Chapter 2

Experimental Description

2.0.3 Overview of Conducted Experiments

Cell Type	MT	BM	Gtom	CM
MCC13/HaCaT	x	x	x	x
rLSEC	x			x

x indicates conducted experiments

Abbreviations

MT MitoTracker
MTdr MitoTracker Deep Red
MTG MitoTracker Green
BM CellLight Mitochondria-RFP, BacMam 2.0
Gtom GFP targeting mitochondrial outer membrane protein tom20
CM CellMask
CMdr CellMask Deep Red
CMO CellMask Orange
MCC13 Human skin cell line from Merkel cell carcinoma
LSEC Liver sinusoidal endothelial cell

2.1 Mapping Mitochondrial Regions

This section describes the methods for labeling mitochondria with three different probes (Gtom, BM and MTdr) and optimization for time-lapse (TL) imaging with MTG.

Growth of cell lines

MCC13 cells were first provided by the Vascular Biology Research Group, and HaCaT cells provided by the Drug Transport and Delivery Research Group. They were grown in cell medium made up of 89% RPMI or DMEM, 10% fetal calf serum (FCS) and 1% antibiotics to prevent growth of bacteria, and kept in an incubator at 37 °C and with 5% CO_2. Cells had to be divided twice a week to avoid overpopulation.

Transfection of cells using Lipofectamine

The following was done: Bacterial stabs for growing Gtom and Btom plasmids were bought from Addgene (plasmid numbers 54282 and 55328). Bacterial colonies were grown and the pDNA was purified using Miniprep (Thermo Scientific GeneJET Plasmid Miniprep Kit) according to protocol, and the final pDNA concentration measured using NanoDrop. Plasmids could then be stored for long periods of time in the freezer before being used.

Cells were transfected with the purified pDNA using Lipofectamine 3000 according to the manufacturer's protocol. This type of transfection had to be carried out at least two days before imaging to allow the cells to incorporate and produce suitable amounts of the FP encoded for, and was likely to kill a large percentage of the targeted cells. The cell death rate during transfection was also highly dependent on how long the cell lines had been cultivated in the lab after thawing. To reduce stress on recently transfected cells they were grown in antibiotic-free medium.

Staining with CellLight Mitochondria-RFP BacMam 2.0 (BM)

Staining with BM has to be done at least 16 hours before imaging to allow the cells to generate the FPs encoded for by the BM transduction. If too much time is allowed to pass (more than 24 hours, dependent on cell type) the cells are likely to lose the FPs. Imaging of BM was therefore done 16-24 hours after staining/adding the transduction reagent. The cells were plated in MatTek dishes at 40-50 % confluency and transfected according to the probe's protocol with concentrations ranging from 15 to 45 PPC (particles per cell).

Optimization of MitoTracker Green (MTG) for time-lapse

Experiments were done to determine optimal staining conditions (concentration and incubation time) for time-lapse (TL) for the MCC13 cell line with MTG.

Criteria for Optimality
a) Few morphological artifacts
b) High number of frames of 3D-SIM possible before destructive photobleaching (not obtaining satisfactory SIM reconstruction)

Staining Titration
To determine the optimal staining protocol with MTG we did the following experiments on MCC13s:
Cells were seeded on coverslips the day before imaging, and incubated at 37C in 5% CO2. Concentrations of MTG were added in the range of 10-400 nM and incubation times ranged from 15-45 minutes. MTG incubation was followed by double washing and imaging in live cell imaging medium (purchased from Thermo Fisher). Imaging was performed immediately after labeling and done at room temperature ($\approx 24\,^{\circ}\mathrm{C}$).

Imaging Parameters
At the same time as staining optimization, the microscope imaging parameters were also optimized following the same criteria for optimality: 1) Illumination intensity (%T)
2) Exposure time per 2D image (in ms)
3) Time between each (3D) frame
4) Total stack size (µm): one 2D plane needed to be imaged for each 125 nm of sample thickness in the z-direction (along the optical axis of the microscope)
5) Immersion oil refractive index

To accomplish satisfactory SIM reconstruction (with resolution of 100-130 nm and little/no artifacts) the maximum intensity count is used to indicate sufficient signal, but this is very sample-dependent and can vary depending on background signal, very bright spots in the sample, and other factors. Typically for MT under suitable staining conditions around 2000 counts was found to be the lower limit for good reconstruction. Increasing both 1) and 2) increased the intensity count, but increasing 1) resulted in quick bleaching compared to increasing 2) (for comparable intensity counts). Usually 1% laser transmission (%T) with 12 ms exposure time was suitable and optimal for MTG.

The time between each 3D frame was found to have little effect on either 1) or 2), but larger stack sizes (in z) gave quick bleaching and reconstruction artifacts. 1-3 µm was normally used, with 1 µm for dark, quickly bleaching or very thin samples, and 3 µm for thick and bright samples.

Optimizing the immersion oil is really optimizing the PSF of the imaging system. This has to be done because the reconstruction algorithm assumes a certain PSF which changes with e.g. wavelength, temperature, distance from coverslip, coverslip thickness, immersion medium of sample. This is solved by changing the refractive index of the immersion oil on the microscope objective. If not optimized, reconstruction artifacts are likely (discussed further in section 3.3).

Staining with MitoTracker Deep Red (MTdr)

Incubation/staining with MT should be done right before imaging since the cell is likely to be damaged by MT after extended periods of time and will also lose the staining after some hours. For combined experiments with the FPs, MT incubation had to be done as the last step. The concentration was tested in the range of 5-400 nM. 75-100 nM with 30 min incubation time was found suitable (for non-transfected cells) if washed 4 times in an appropriate buffer- solution (PBS or live cell imaging medium). Fewer than 4 times washing led to strong background signal for SIM.

2.2 Liver Sinusoidal Endothelial Cells

This section describes the sample preparation for obtaining dually-stained rat liver sinusoidal endothelial cells (rLSECs) using MTG and CMdr for TL imaging of fenestration dynamic.

Staining with MitoTracker and CellMask Deep Red

The same staining parameters that were optimized for MCC13 cells were tested for LSECs and found to be suitable. For dual-staining with CMdr, cells were first incubated with MTG for 20 minutes before CMdr was added for co-incubation for an additional 10 minutes. The samples were washed three times in live-cell imaging medium and imaged with 3D-SIM. The CMdr staining was found appropriate without further optimization experiments. Optimization for TL was done with similar criteria as discussed in previous section, but now with a focus on fenestration dynamic:

Optimization Criteria
a) Resolvable fenestrations without artifact.
b) Fenestration dynamic.

The results are presented and discussed in section 3.2.

Chapter 3

Results and Discussion

3.1 Mapping Mitochondrial Regions

This section presents results from *the mapping of mitochondrial regions*, meaning imaging experiments with the goal of *visualizing* different (and specific) mitochondrial structures. This was done *in living cells* utilizing spectrally separated probes believed to target different mitochondrial regions.

First, mitochondria are labeled and imaged using the three different probes (introduced in section 1.3.2) and 3D-SIM. The resulting super-resolved images are then structurally compared. Subsequently, the probes are applied together for dual color experiments to confirm the apparent structural differences between the probes (in mitochondria with very varied morphology). These experiments showed that it is necessary to re-optimize the staining parameters when multiple probes are applied simultaneously compared to applied individually.

When all the three (spectrally separated) probes have been applied together in dual-color imaging with SIM (at super-resolution), they are all applied together showing three different structures of mitochondria at once (in living cells). This highlights the strength of the gained optical resolution from SIM coupled with the specific labeling of subcellular structures using fluorescent probes.

Finally, time-lapse (TL) experiments are done on all probes individually and challenges with the SIM technique discussed. Combining SIM with diffraction-limited *deconvolution microscopy* (DV) allowed for the study of mitochondrial dynamics with *low light exposure* and *high frame rate*. Since the OMX uses same stage for both SIM and DV, dynamics can be followed over a large field of view with low phototoxicity and then high resolution (light intensive) snap-shots can be acquired on a few selected points of interest.

3.1.1 Mitochondrial Outer Membrane using Gtom

To visualize the outer membrane of mitochondria, cell lines (MCC13 and HaCaT) were transfected (as described in Ch. 2.1), resulting in cells with fluorescently labeled mitochondria. More specifically, the mitochondrial outer mem-

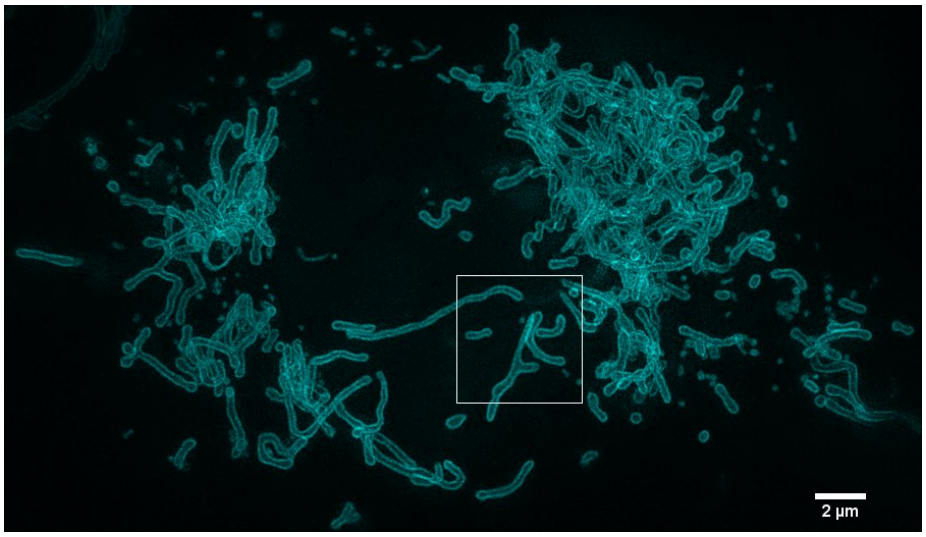

Figure 3.1: *MCC13 transfected using Gtom* (λ= 488 nm). The image is a maximum intensity projection of 3D-SIM data, and the square indicate the origin of the next two figures.

brane protein tom20 was labeled with GFP (Gtom), with excitation wavelength (ex. λ) 488 nm. The same was tried (and accomplished) for a different FP (BFP with ex. λ= 405 nm), but the GFP label was found to be much brighter than the BFP, and hence, more suited for SIM. Therefore only Gtom was pursued for time-lapse and for multiple-color experiments.

One example of a cell with mitochondria brightly labeled with Gtom is shown in Figure 3.1. The darker area in the middle is where the nucleus is (for recap on cell anatomy, see Figure 1.8). A magnified view of the area in the square (this time only a single slice from the z-stack) is shown in Figure 3.2 with a (diffraction-limited) deconvolution microscopy (DV) comparison (acquired right after the SIM image). From the SIM image (B) it looks like the GFP really is distributed on the mitochondrial outer membrane, while DV (A) does not provide this information; It is beyond the resolution limit for conventional microscopy. To emphasize the higher resolution provided by SIM, also a line profiles of DV(**A**) and SIM (**B**) is provided in Figure 3.3.

3.1.2 Mitochondrial Matrix using BM

To image the mitochondrial matrix (inside the mitochondrial *inner* membrane), cells were transduced with *CellLight Mitochondrial RFP* (BM) as described in section 2.1. The cells displayed high transduction efficiency for all concentrations of BM tried (range 15 to 45 PPC) after 16-24 hours incubation. An example of a cell brightly expressing RFP (ex. λ= 568 nm) in the mitochondrial matrix is shown in Figure 3.4. We can see that mitochondria visualized through this

Figure 3.2: *DV-SIM comparison of mitochondria labeled with Gtom.* Single z-plane images obtained with **A**: Deconvolution microscopy (DV) and **B**: SIM. Scale bar 0.5 µm.

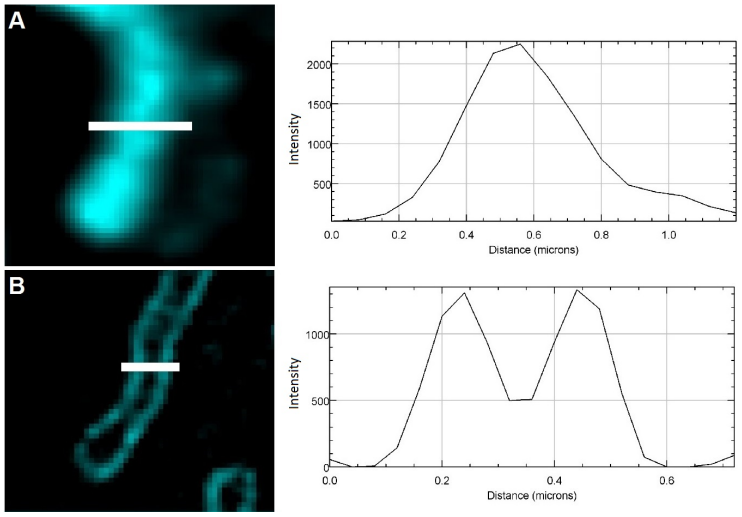

Figure 3.3: *DV-SIM comparison of Gtom with line profiles.* **A**: DV and **B**: SIM. Single z-plane images; plots of the intensity along the indicated line on the left are shown to the right of the corresponding image. With diffraction-limited microscopy, Gtom (ex. λ= 488 nm) seems to be labeling the entire mitochondrion, while with the additional resolution provided by SIM Gtom seems to be localized around an internal compartment.

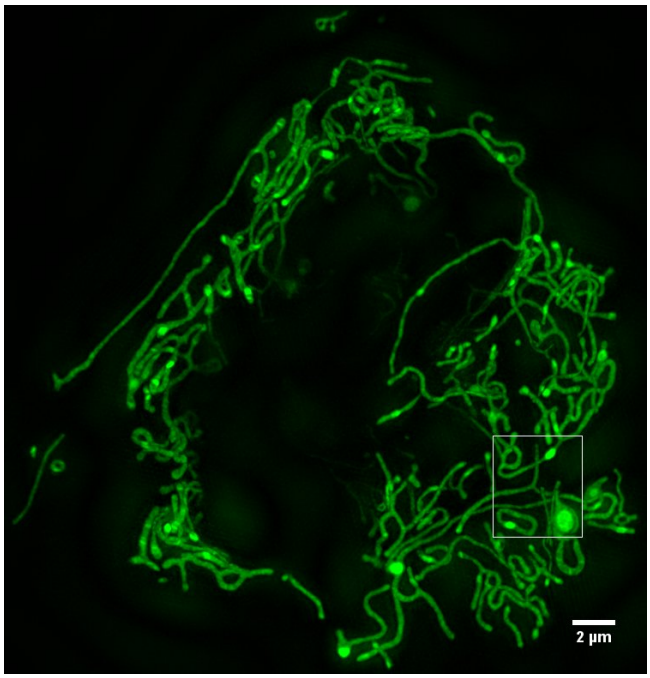

Figure 3.4: *MCC13 cells transduced using BM* (ex. λ= 568 nm). Projected 3D-SIM image, the square is shown magnified in the next figure.

probe appear as a complex network of thin strings (very different from Gtom), but also 'blobs' of RFP were frequently encountered (including in the images shown). The mitochondria were more prone to 'blobbing' when transduced with higher concentrations of BM, and the blobbing is likely to be an artifact of the labeling method (over-expression of RFP-labeled protein).

The indicated square in Figure 3.4 is shown magnified in Figure 3.5 with the SIM image on the left and a conventional wide-field microscopy (WF) image on the right. From this SIM-WF comparison we can see that SIM provides extra detail about the complex distribution of mitochondria compared to diffraction-limited microscopy.

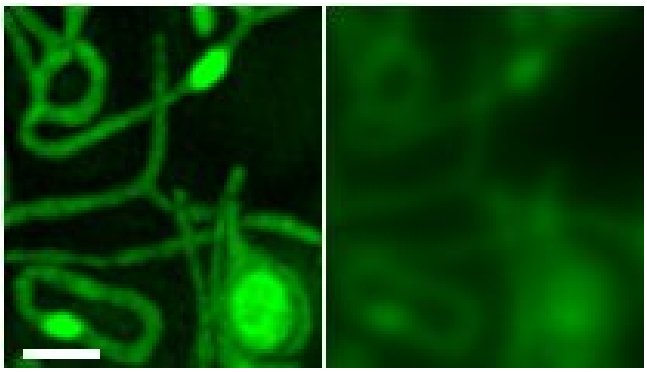

Figure 3.5: *SIM-WF comparison of BM* (ex. λ= 568 nm) in a MCC13 cell. The thin lines and blobs resulting from BM is detectable also using diffraction-limited microscopy, but SIM provides extra detail about the complex network of mitochondria. Projected 3D-images, scale bar 1 µm.

3.1.3 Mitochondrial Intermembrane Space using MTdr

To visualize the mitochondrial intermembrane space (MIS), between the mitochondrial outer membrane (MOM) and matrix (inside the mitochondrial inner membrane (MIM)), cells were incubated with MitoTracker Deep Red (MTdr) (ex. λ= 642 nm) as described in section 2.1. Figure 3.6 shows a projected 3D-SIM image of two closely attached MCC13 cells incubated with 75 nM MTdr for 30 minutes, which was the staining protocol found to be optimal. The optimization of the MitoTracker (MT) staining protocol will be discussed in later sections (3.1.4 and 3.1.6).

The square indicated in Figure 3.6 shows from where the next images are taken. Figure 3.7 shows single slices from the acquired 3D-data of both DV (top) and SIM (bottom), with plotted line profiles of the regions indicated. This shows that SIM provides sufficient resolution to reveal sub-mitochondrial structures not resolvable with diffraction-limited DV.

Three-Probes Summary

Three different mitochondrial probes targeting different structures and with spectral separation (as shown in the staining sketch in Figure 1.9) have been individually applied and optimized for super-resolution imaging with SIM. The results are summarized in Figure 3.8, where (**A**) the mitochondrial matrix is labeled with BM (ex. λ= 568 nm), (**B**) the intermembrane space is targeted with MTdr (ex. λ= 642 nm) and (**C**) the mitochondrial outer membrane with Gtom (ex. λ= 488 nm). They do indeed look structurally different, but due to high variability in mitochondrial morphology, co-staining should also be applied to confirm distinguishable localizations.

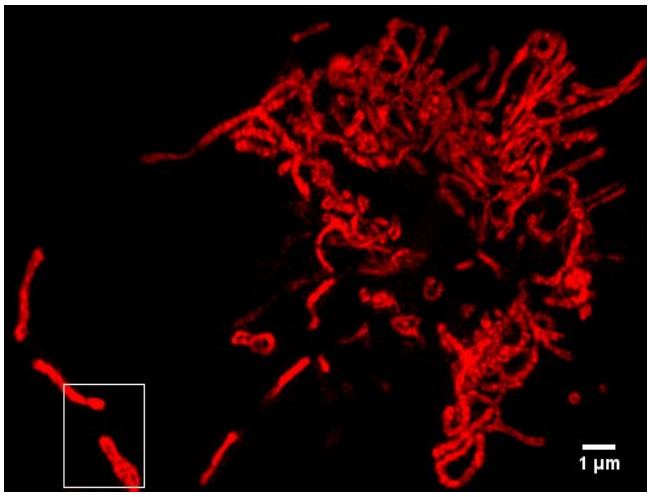

Figure 3.6: *MCC13 cells labeled with MitoTracker Deep Red* (ex. λ= 642 nm). Projected 3D-SIM image, the next figure originates from the indicated square.

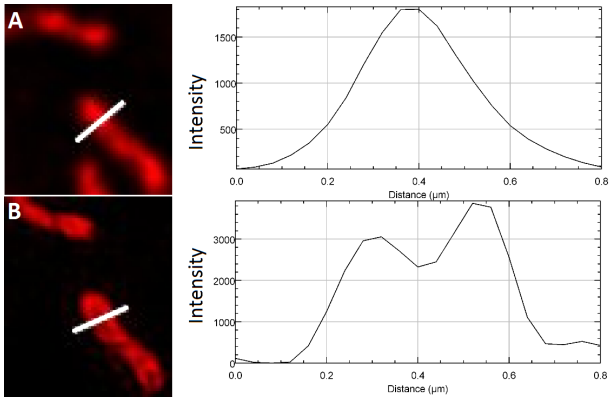

Figure 3.7: *DV-SIM comparison of mitochondria labeled with MTdr* (ex. λ= 642 nm). **A**: DV, **B** SIM. Both are single slice images. The indicated line profiles are plotted to the right. The 2X resolution enhancement provided by SIM enables additional structures to be resolved.

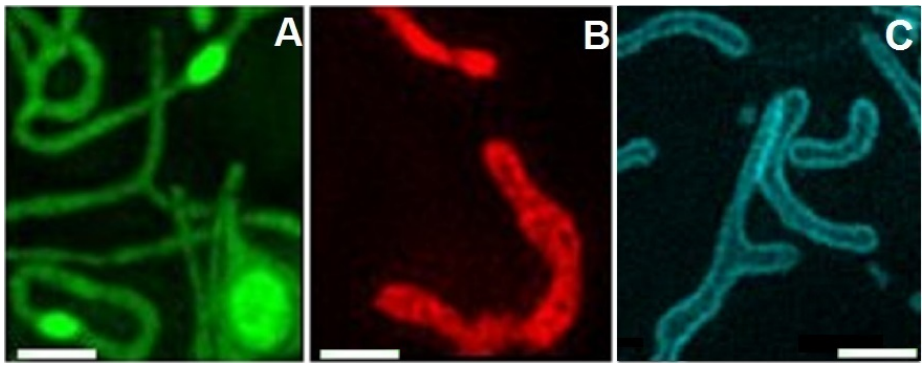

Figure 3.8: *Comparison of MTdr, Gtom, and BM mitochondrial labels.* BM (**A**) localizes inside the mitochondrial inner membrane, MTdr (**B**) between the mitochondrial inner and outer membranes, and Gtom (**C**) labels the mitochondrial outer membrane. Projected 3D-SIM images. Scale bars 1 µm.

3.1.4 Dual-Color Labeling

The three probes targeting different mitochondrial regions, applied and optimized individually in the previous section, will here be applied together two and two and compared. This is possible because of their different fluorescence excitation/emission spectra (introduced in section 1.1.2), which allows for only exciting and detecting one of the probes at the time. Referring to Figure 3.8, the following combinations are shown subsequently: **A** + **C**, **B** + **C** and **A** + **B**.

Combining Gtom and BM

When combining the two transfection methods for fluorescent mitochondria, cells were first transfected with Gtom because of the longer timescale and higher death-rate for this transfection method (described in section 2.1). The cells were then given some time to recover (2-5 days) and reach the desired confluency (cell density, 40-60% in this case) for the second transfection with BM.

Mitochondria from cells strongly expressing both FPs (Gtom ex. λ= 488 nm and BM ex. λ= 568 nm) is shown in Figure 3.9, with the two color-channels first alone and then combined. From this, it is apparent that the probes indeed are located on different mitochondrial structures: Gtom (**A**, in cyan) is located on the mitochondrial outer membrane and BM (**B**, shown in yellow) is inside of the outer membrane.

The dual-transfection experiments revealed that cells transfected *once* with Gtom (and strongly expressing GFP), were less likely to have generated large amounts of the second fluorescent protein, RFP, as shown in Figure 3.10. Image **A** shows the green channel (ex. λ= 488 nm) with a Gtom transfected cell (point 1 in the figure), image **B** shows the orange channel (ex. λ= 568 nm)

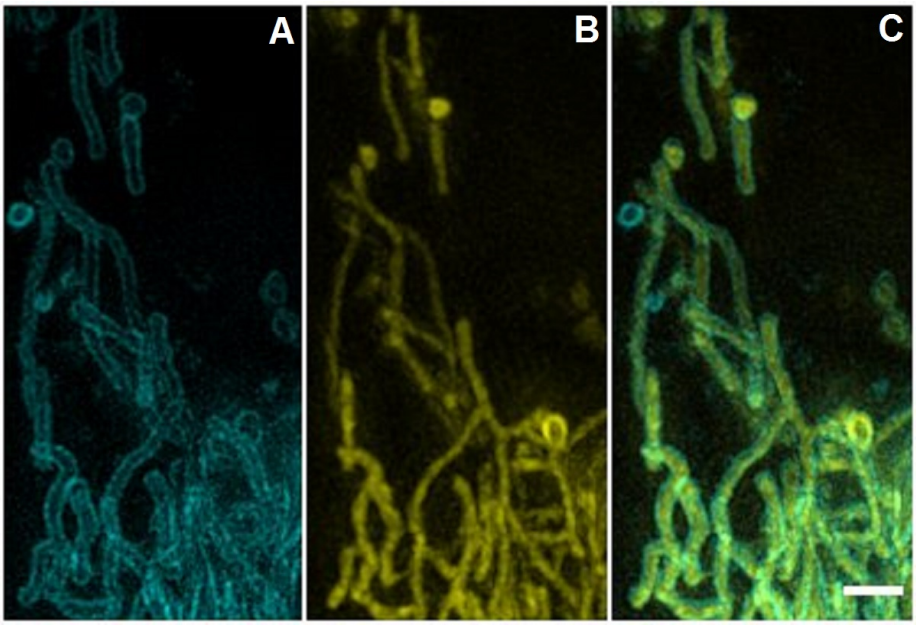

Figure 3.9: *A subsection of an MCC13 cell labeled with Gtom and BM.* Projected 3D-SIM images, **A**: Gtom (ex. λ= 488 nm), **B**: BM (ex. λ= 568 nm), **C**: **A** + **B** combined. Scale bar 1 µm.

with BM transduced cells expressing RFP (points 1-4 in the figure), and image **C** shows both channels combined. The Gtom transfected cell (1) is expressing less RFP (from BM) than cells 3 and 4, which have not produced Gtom. cell 3 and 4 which has not produced Gtom. Cell 2 has not produced GFP (from Gtom), but still only expresses a small amount of RFP (from BM). The method of transfection for introducing foreign DNA into cells is notorious for producing variable expression levels. Additionally, cells transfected *once* seemed less likely to become transfected a second time (by BM) compared to non-transfected cells. However, the only information available from the images is relative amounts of FPs, so it is possible that cells have been transfected by both methods (incorporated DNA for producing both FPs), but only had time/resources to produce the first type of FP.

Because of the low expression level of BM in Gtom transduced cells, the optimal amount of BM for transducing already transfected cells was higher than for transducing non-transfected cells.. However, increasing the amount of transducing agent was not strictly necessary for finding a dually transfected cell. Probing by transfection is in this quite different from staining with MT, as will be shown towards the end of this section.

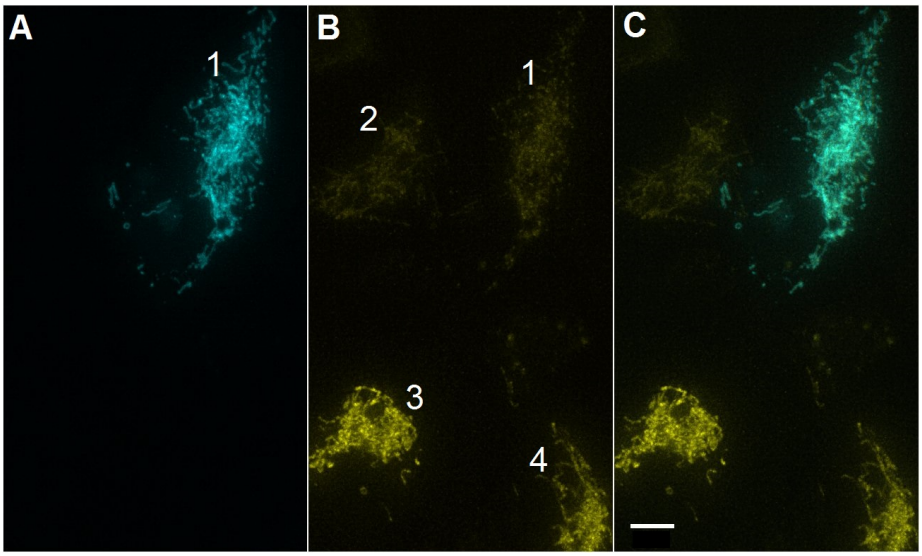

Figure 3.10: *Variable expression levels of fluorescent proteins.* **A**: Green channel (ex. λ= 488 nm) with a Gtom transfected cell (point 1), **B**: Orange channel (ex. λ= 568 nm) with BM transduced cells expressing RFP (points 1-4), and **C**: both channels combined. The Gtom transfected cell (1) is expressing less RFP (from BM) than cells 3 and 4, which have not produced Gtom. Cell 2 has not produced GFP (from Gtom), but still only expresses a small amount of RFP (from BM). However, cells transfected *once* seemed less likely to become transfected a second time (by BM) compared to non-transfected cells. Projected 3D-DV images. Scale bar 5 µm.

Combining Gtom and MT

HaCaTs stably transfected with Gtom (ex. λ= 488 nm) were obtained by methods described in section 2.1. In other words, skin cells with fluorescently labeled mitochondrial outer membrane were proliferating on coverslips ready for dual-color experiments. To, at the same time, visualize the structure of the mitochondrial *inner* membranes, Gtom transfected cells were incubated with MTdr (ex. λ= 642 nm) and their spectral separation allowed for clear differentiation between the two probes. The resulting image is shown as a maximum intensity projection in Figure 3.11 and the indicated square is shown with separate color channels in Figure 3.12. It becomes clear from these figures that MTdr accumulates *inside of* the Gtom-tagged structures.

The MTdr incubation was done as found suitable for non-transfected cells (100 nM for 30 minutes), and this was suitable also for the cells expressing Gtom.

Combining BM and MTdr

Cells (MCC13) transduced with BM (ex. λ= 568 nm) which thus had mitochondria with fluorescent proteins in the mitochondrial matrix (*inside* the inner membrane) were grown on coverslips as described in section 2.1. These were now ready for dual-color experiments by incubation with spectrally separated MTdr (ex. λ= 568 nm). This way, both the mitochondrial matrix *and* the intermembrane space (revealing the structure of the inner membrane) could be simultaneously imaged by SIM.

The BM transduced cells were incubated with the optimal amount of MTdr found previously (75 to 100 nM), and it was found that the BM transduced cells (point 1 in Figure 3.13) displayed greatly reduced retention of MTdr compared to non-transfected cells (also) in the same sample. This is shown in Figure 3.13, where the two color channels are shown alone and combined. The non-transduced cell (1) is brightly labeled with MTdr, while the transduced cells (points 2 and 3) are not.

A closer investigation of the specific target for this transduction agent gives a likely explanation for this. This probe targets the mitochondrial matrix enzyme E1 alpha pyruvate dehydrogenase[36], which is essential in the breakdown of glucose and the release of chemical energy in the form of ATP[37]. Metabolic oxidation of sugar involves the *electron transport chain* (e^-) and a *proton pump* (H^+) resulting in the (negative) mitochondrial transmembrane potential, $\Delta\Psi$.[41]

One should be careful with making conclusions, but it seems plausible that labeling this enzyme with a (at the molecular level) gigantic FP could, at least to some extent, affect its function. Since the accumulation of MT in mitochondria depends on $\Delta\Psi$, it seems like a reasonable assumption that the BM probe is affecting the mitochondrial transmembrane potential, $\Delta\Psi$.

Increasing the concentration of MT helped resolve this issue and enable dual color images of mitochondria. Figure 3.14 shows a projected 3D-SIM image of mitochondria in within a sample of MCC13 cells transduced with BM and

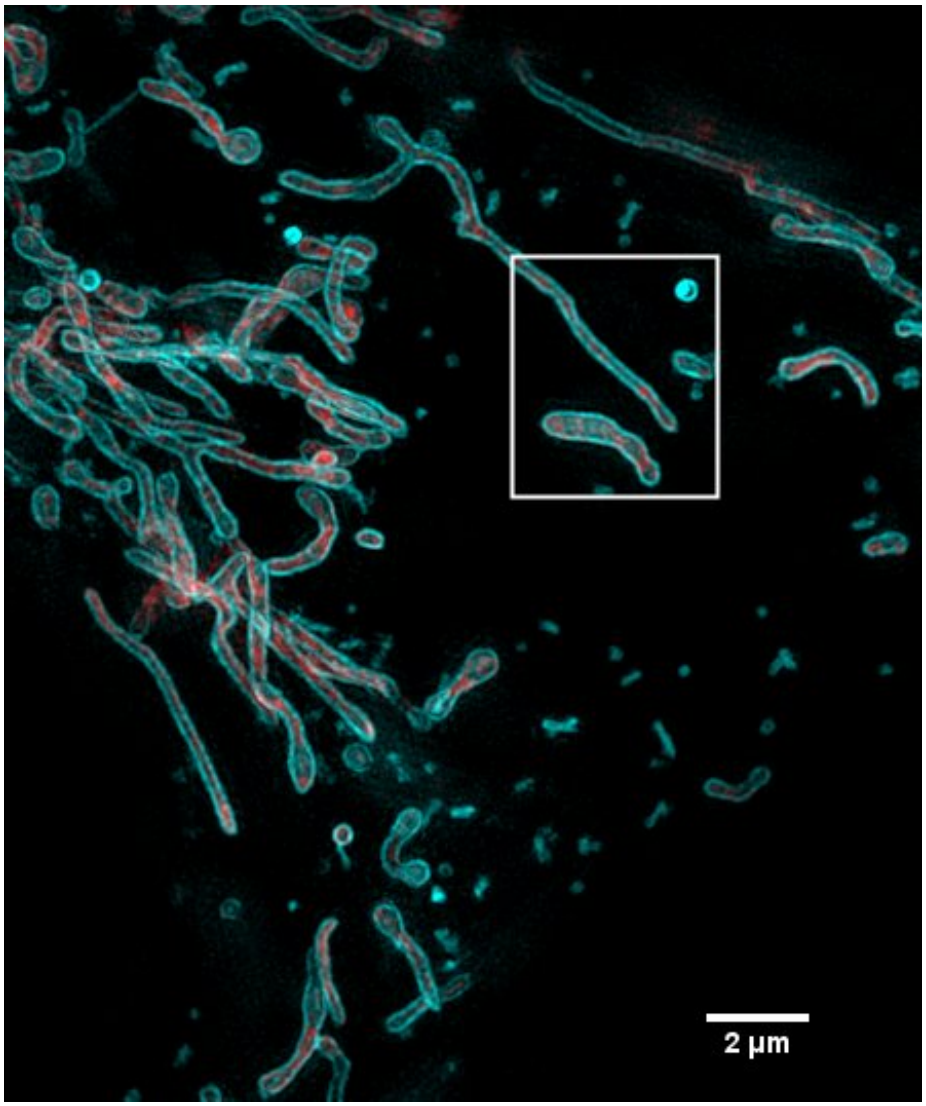

Figure 3.11: *Part of a HaCaT cell labeled with Gtom (ex. λ= 488 nm, in cyan) and MTdr (ex. λ= 642 nm, in red).* Projected 3D-SIM image. The square is further investigated in next figure.

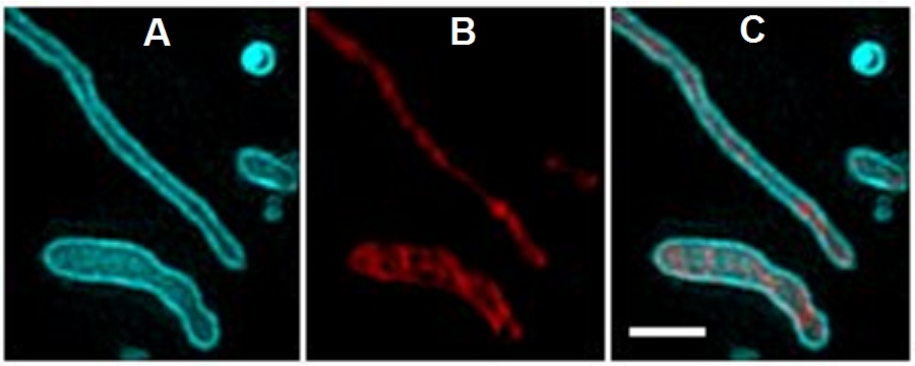

Figure 3.12: *Zoomed in image of mitochondria within a HaCaT cell.* Mitochondria were labeled both with Gtom (**A**) and Mtdr (**B**). **C**: Merged view of **A** and **B** showing the different areas labeled with each probe. Projected 3D-SIM images. Scale bar 1 µm.

stained with 400 nM MTdr. The uppermost square (close to the middle of the cluster/cell) is investigated further in Figure 3.15, where a magnified view is given of the channels alone and combined.

As before, BM (in Figure 3.15**A**) is a complex network of strings, but also many *rings*. MTdr (**B**) labels fewer mitochondria and causes some background signal, as if there was a nucleus there (MTdr tends to also stain the lipid membrane around the nucleus in high concentrations). **C** shows both channels combined, and it seems like only about half of the mitochondria labeled with BM are labeled with MTdr.

The lower square of Figure 3.14 is similarly shown in Figure 3.16. The lower density of mitochondria in this region makes comparison easier. The arrows indicate mitochondria that look the the same with the two probes, while the circles indicate mitochondria with clear structural differences between the two probes.

The reason why probes which target different structures can look the same can potentially be explained as having insufficient resolution to distinguish them in very thin mitochondria. It can also be that (in these mitochondria) MTdr has diffused through also the mitochondrial *inner* membrane and is (as BM) labeling the matrix instead of the intermembrane space. For the mitochondria where the probes resulted in distinguishable structures (circles), MTdr is located both inside and around the rings.

The mitochondrial morphology in this cell cluster was characterized by many rings and very thin rods. It can be an artifact from the BM probe, but also ordinary cell function. For example, the mitochondrion of the *Leishmania tarentolae* (it has only one) becomes circular during normal cell division[48].

The staining with MTdr found suitable for BM transduced cells (400nM to 500nM) was over five times higher than the staining concentration found optimal for non-transduced cells (which was 75-100 nM). Few transduced cells were

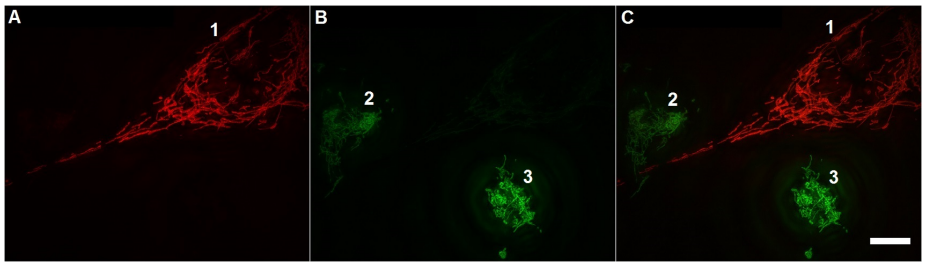

Figure 3.13: *Reduced retention of MTdr in BM-transduced MCC13 cells.* Cell 1 is brightly labeled with MTdr but not with BM, cells 2 and 3 are labeled with BM but not with MTdr. **A**: MTdr (ex. λ= 642 nm), **B**: BM (ex. λ= 568 nm) and **C**: previous combined. Projected 3D-SIM images. Scale bar 10 µm.

brightly labeled even with these enhanced staining conditions, but increasing further to 1000 nM showed extensive staining of the entire cell, lowering the contrast to the extent of making the mitochondria indistinguishable from the rest of the cell. High concentrations of MTdr also causes morphological (and most likely functional) artifacts in that they lose the rod-like shape and look more like dead sacks of stain. This is exemplified in Figure 3.17 which shows mitochondria in MCC13 cells labeled using BM and co-stained with 1000 nM MTdr, and are not looking healthy, most likely from overstaining and/or BM transduction. MTdr in large concentrations stains the entire cell which gives too much background signal for imaging mitochondria, but the combination with BM enables recognition of the morphological artifacts, which are discussed further in section 3.1.6.

3.1.5 Combining Three Probes

To really test the new nanoscope, three-color imaging of mitochondria was performed. This was done by applying all three probes together: Gtom (ex. λ= 488 nm), BM (ex. λ= 568 nm) and MTdr (ex. λ= 642 nm).

To achieve labeling of mitochondria with all three probes, the labeling order and timing was crucial. As described in section 2.1, the cells (MCC13) were first transfected with Gtom and then left to produce this FP (ex. λ= 488 nm) for at least two days. Subsequently, the cells were labeled by a second FP using BM (ex. λ= 568 nm). For this (virus-mediated) transduction, 16-24 hours incubation was suitable. In the end, right before imaging, MTdr incubation was done for 25-30 minutes with 500 nM providing the best results. Labeling with MTdr at an earlier stage would have been harmful to cell health and also allowed the MTdr to diffuse *out* of the mitochondria, so the specific order and timing had to be like it was.

A projected 3D-SIM image of mitochondria labeled with all three probes is shown in Figure 3.18 with each of the color channels shown separately and

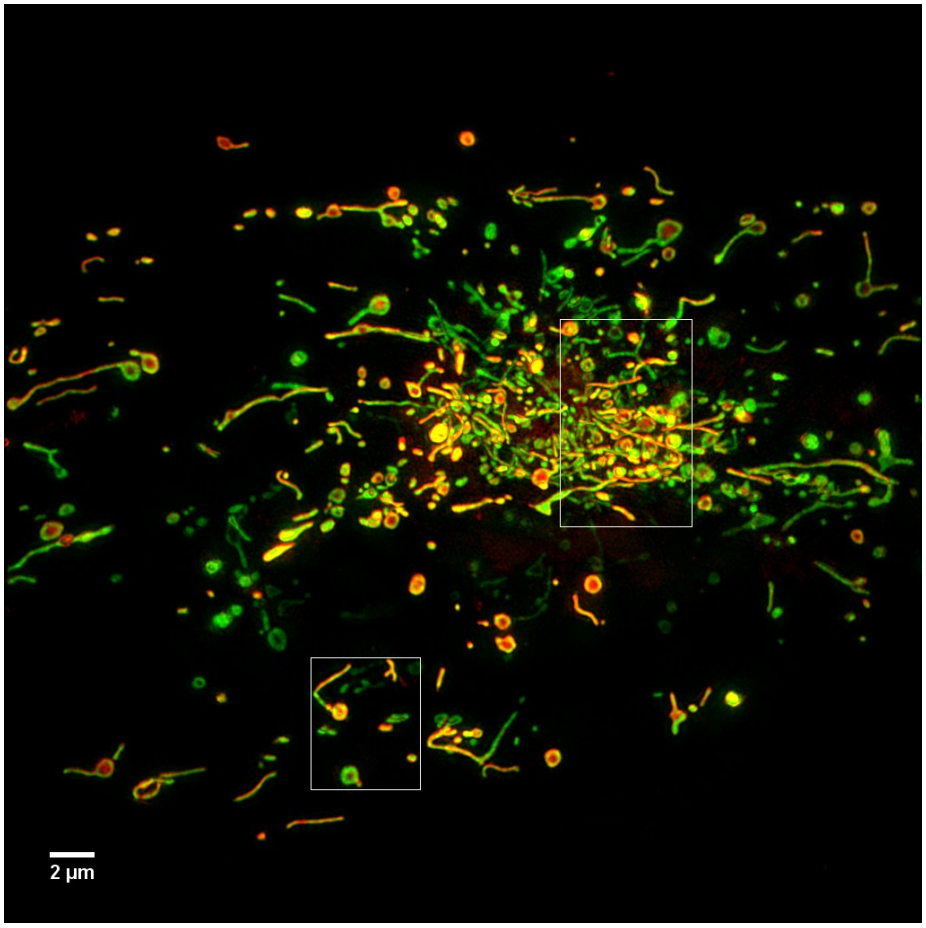

Figure 3.14: *MCC13 stained with BM (ex. λ= 568 nm, in green) and MTdr (ex. λ= 642 nm, in red).* Mitochondria display very varied morphology and retention of MTdr. The squares are investigated further in the next figures. Projected 3D-SIM image.

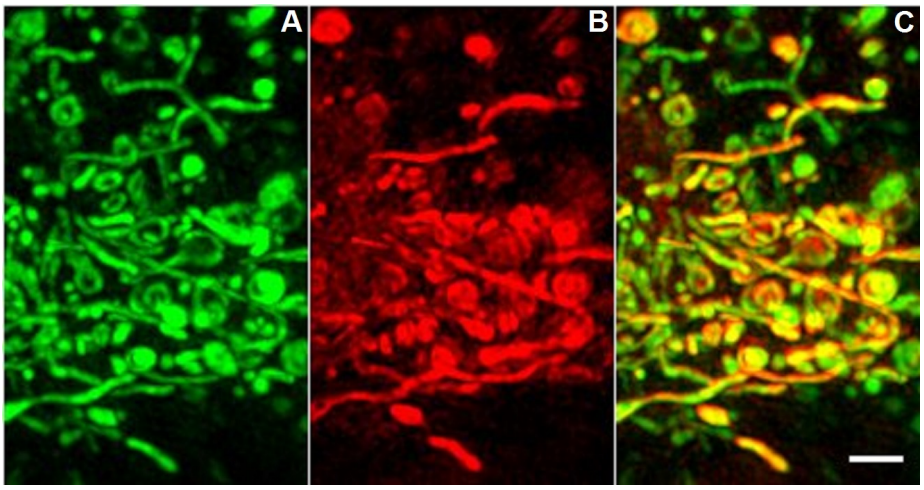

Figure 3.15: *Mitochondria in a MCC13 cell stained with BM and MTdr.* Projected 3D-SIM images. **A** BM (ex. λ= 568 nm), **B** MTdr (ex. λ= 642 nm), **C**: previous combined. BM is a complex network, while MTdr stains fewer mitochondria and also gives some background. Scale bar 1 µm.

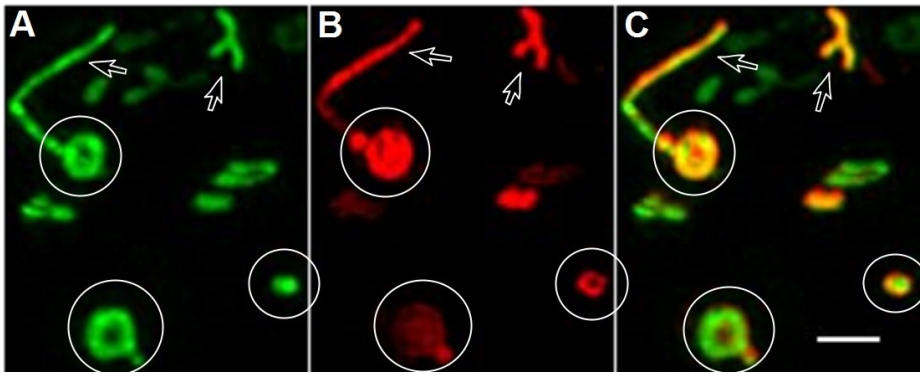

Figure 3.16: *Mitochondria in a MCC13 cell labeled with BM and MTdr.* Projected 3D-SIM images. **A**: BM (ex. λ= 568 nm), **B**: MTdr (ex. λ= 642 nm), **C**: previous combined. Arrows indicate structures looking similar, while circles indicate structural differences between the two probes. With the available resolution (120-130 nm) the probes appear in some places to be co-localized. Scale bar 1 µm.

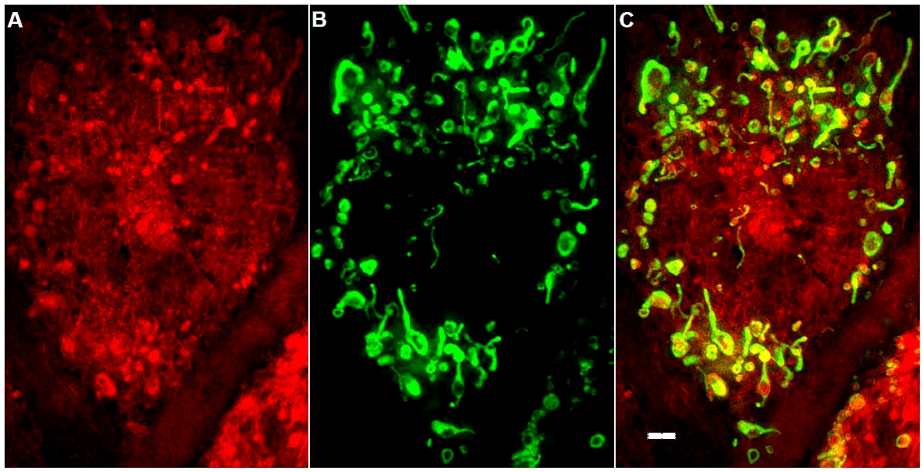

Figure 3.17: *Morphological artifacts from overstaining with MTdr in BM-labeled MCC13 cells.* Reduced retention of MT in BM-labeled cells required higher concentrations of MTdr to achieve similar intensities, but too much MTdr (**A**) stains other cellular structures and causes morphological artifacts (**B**). **A**: MTdr (ex. λ= 642 nm), **B**: BM (ex. λ= 568 nm), **C**: **A** and **B** combined. Scale bar 2 µm.

combined. The bottommost mitochondrion is shown magnified in Figure 3.19 with separate color channels (single slice from the 3D-SIM image) and Figure 3.20 shows these channels projected with a staining-sketch comparison.

The resolution is at the limit for the SIM system, but the plan seems to have worked: the mitochondrial outer membrane is labeled with Gtom (ex. λ= 488 nm), the matrix is labeled with BM (ex. λ= 568 nm) and the intermembrane space is stained with MTdr (ex. λ= 642 nm). Even though the labels in many (or most) places are closer together than 100 nm, they are still distinguishable due to their structural differences, as is clear from Figure 3.19. To the best of our knowledge, mitochondria has never been resolved simultaneously with three different probes in living cells before.

3.1.6 Time-Lapse

Time-lapse (TL) imaging is the microscopy-equivalent of movie-making. It is a valuable tool to study *cellular function and processes*, as opposed to the mere structural information provided by 'single-shots'.

Many TL experiments were done with 3D-SIM in an effort to follow mitochondrial dynamics at SR. Because of quick bleaching (of all probes), the intensity was kept as low as possible, extending the amounts of frames possible before the sample was completely bleached. By lowering the intensities too much (typically s/n below 10/1), the point of using SIM diminished with

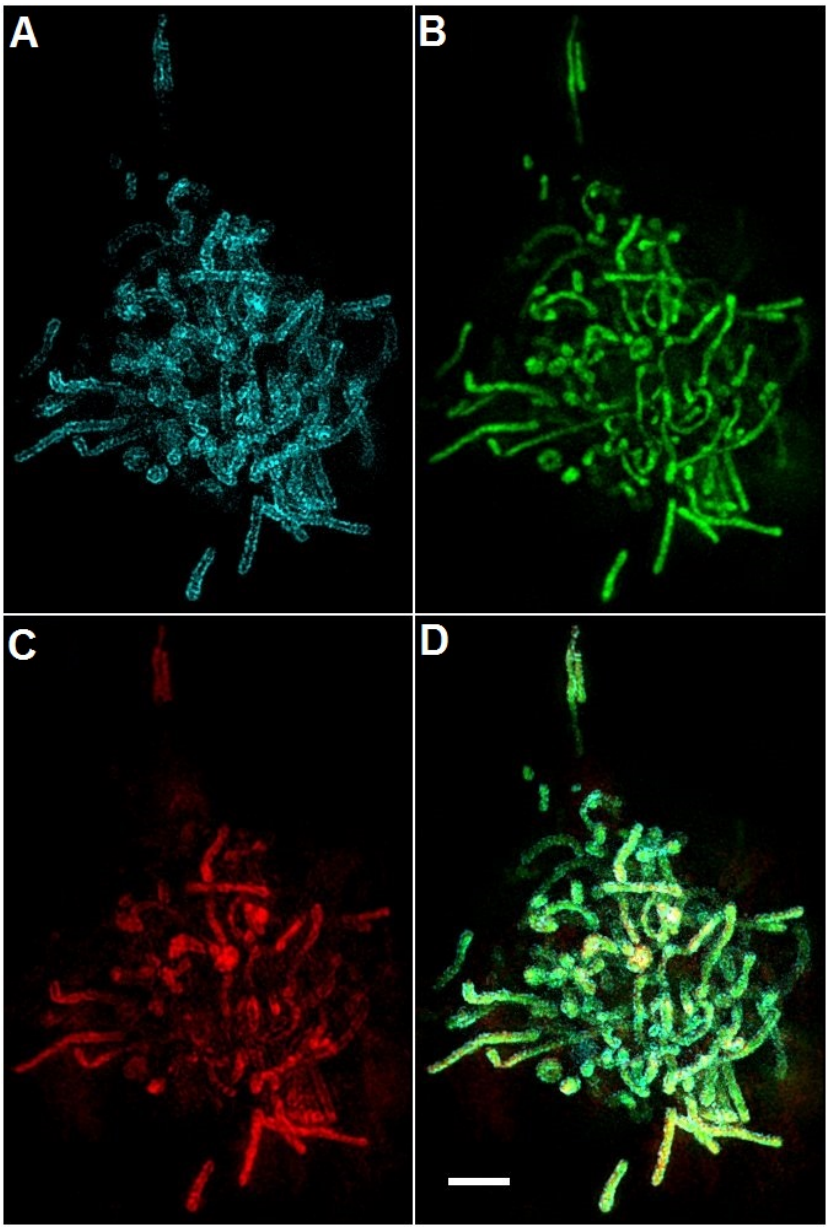

Figure 3.18: *All three probes combined in a MCC13 cell.* Projected 3D-SIM images of mitochondria labeled with **A**: Gtom (ex. λ= 488 nm), **B**: BM (ex. λ= 568 nm), **C**: MTdr (ex. λ= 642 nm) **D**: combined. Scale bar 2 µm.

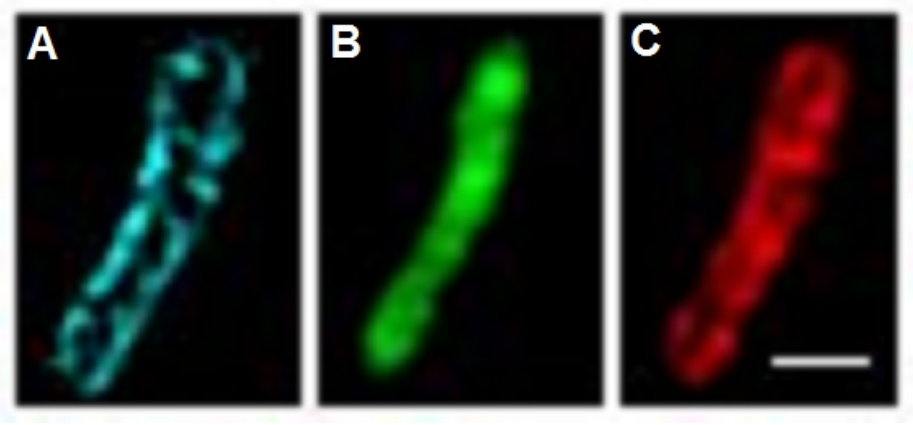

Figure 3.19: *Magnified view of a single slice from previous 3D-SIM image.* **A**: Mitochondrial outer membrane labeled using Gtom (ex. λ= 488 nm), **B**: mitochondrial matrix labeled using BM (ex. λ= 568 nm), and **C**: mitochondrial intermembrane space stained using MTdr (ex. λ= 642 nm). Scale bar 500 nm.

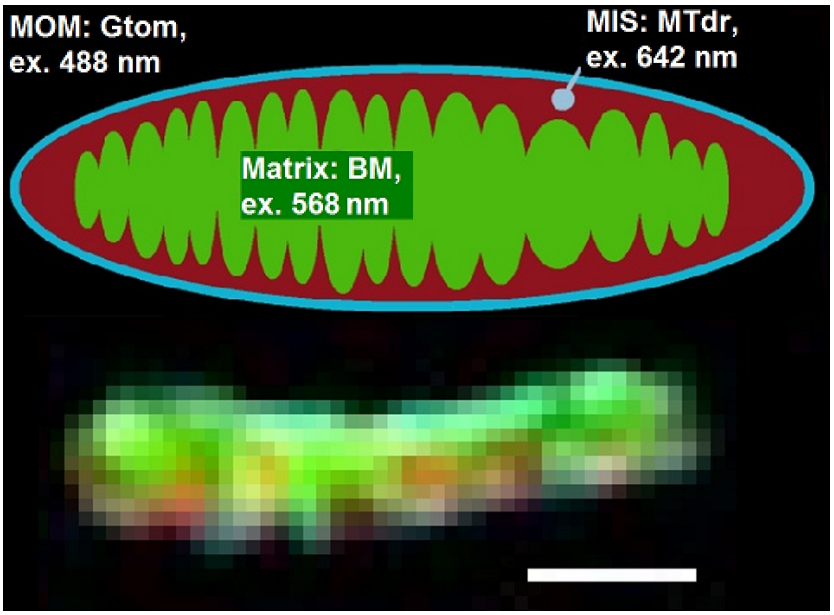

Figure 3.20: *Comparison of tricolor sketch and result.* The resolution required to distinguish all the three probes *at the same time* is at the limit of the SIM system (110-130 nm). Each square (pixelation) of the bottom mitochondrion corresponds to a reconstructed image pixel of 40 nm. Scale bar 500 nm.

the resolution and reconstruction artifacts became obvious (discussed in section 4.3).

Among the probes for mitochondria tested, MT was the best suited for time-lapse in that it was bright enough to obtain most 3D-SIM images before the structures were unresolvable from photobleaching. However, some suspect behavior of the mitochondria was noticed, especially after incubation with high concentrations of MT. The effect was soon named *sphering*, and Figure 3.21 illustrates why. It is a time-lapse of mitochondria stained by a relatively high concentration of MT. In the course of about 24 seconds, the uppermost mitochondrion goes from elongated to spherical; this effect has been confirmed to be three-dimensional. Every mitochondrion did not turn into spheres during this time-lapse, and in fact all behaved a bit differently, but the effect seems to be general in the sense that they become wider and shorter.

No good explanation for this was found in the literature, but there seems to be a common belief that mitochondria are spherical. This is likely because most studies of mitochondrial morphology have been done on fixed/dead cells, and when the mitochondria die (e.g. during the sample preparation for electron microscopy) they sphere-up and obtain the characteristic raisin-shape found in textbooks on cell biology.

It seems plausible that the accumulation and excitation of positive ions (MT) inside of mitochondria could generate destructive amounts of ROS (introduced in section 1.3.2), causing degeneration of structural support, leading to the morphological artifacts. Sphering was not observed by the other probes (unless combined with MT), but poor photophysical properties (combined with light intensive 3D-SIM) also makes many time-points (TP) difficult.

Movie 1 shows a 3D-SIM TL (projected 2 µm stack) of mitochondria stained with Gtom, 6 time-points acquired every 10 seconds, both unprocessed to the left and a (simple ratio) bleach corrected version on the right-hand side. This illustrates the quick bleaching, but also that some dynamics are possible to follow at SR.

Combining SIM with DV Time-Lapse

Because of the challenges with using SIM for TL of mitochondria (or at least with the probes tested), TL was also acquired with deconvolution microscopy (DV). DV proved to be a much better tool for the purpose of monitoring mitochondrial motion. It provides just enough resolution and a larger field of view (including in z-direction), and fewer frames (per 3D-image) makes it quicker and less prone to bleaching. This allowed for long TL of all three probes without bleaching (or sphering) being a big issue. Movies 2, 3 and 4 show long comparable time-lapse of the same three probes tested for SIM, but here much larger stacks (7-8 µm) and images acquired every 30 second for 20-30 minutes. Mitochondria show vigorous movement stained with all probes, so the probes might be less invasive to mitochondrial function than they appear to be while under the harsher imaging conditions with SIM.

The mitochondria displayed considerable dynamics also on a much shorter

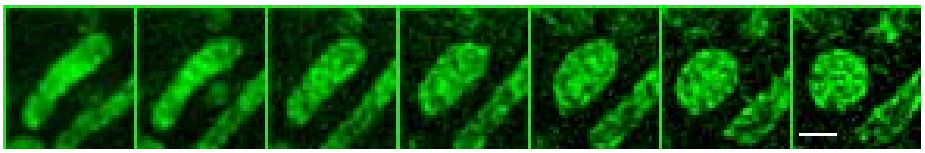

Figure 3.21: *Sphering of mitochondrion within a MCC13 cell with repeated light exposure.* Projected 3D-SIM time-lapse of MCC13 cells labeled with 400 nM MTG. The time-lapse has 4 seconds between each image, and the photobleaching has been adjusted for by gradually increase of intensities. High concentrations of MTG allowed for more frames to be acquired before the sample became too dark to image using SIM, but caused morphological artifacts. Scale bar: 0.5 µm.

timescale. Movie 5 shows a DV TL with images acquired every 5 seconds for 2.5 minutes (30 TP) of a 5 µm projected z-stack. A 3D-SIM image (3 µm projection) of the same cell acquired right before the DV time-lapse is shown in Figure 3.22. The SIM image provides additional resolution, and the DV TL the dynamics. Some selected time-points from the DV TL are shown in Figure 3.23, with the arrows indicating a dividing mitochondrion.

Because of the high photon cost of resolution (of today's optical nanoscopes), live-cell studies with optical microscopy should be performed with as little resolution as strictly necessary for the one's investigation to minimize cell damage and photobleaching. By combining several microscopy options on the same stage (as the OMX's combined DV-SIM), one can tailor the resolution to what is most suitable in each moment of one's (live-cell) study. Many biological events take place on a very broad scale (both in space and time), making the preferable tool for biological research an optical imaging platform with flexible choice of resolution (and hence) microscopy technique.

3.2 Liver Sinusoidal Endothelial Cells

While the main focus of this thesis was studying mitochondria, the nanoscopy group was collaborating with the Vascular Biology Research Group (VBRG) at the Department of Medical Biology. The cells that were made available for this master's thesis were liver sinusoidal endothelial cells (LSECs). Therefore, some of the initial experiments on testing mitochondrial stains for SIM were done on LSECs (as discussed in 3.2.2). However, VBRG was also interested in the function of the cells, so experiments looking at the cell membrane were also done (as discussed in 3.2.1). LSECs are thin cells that line the blood vessels of the liver while acting as a filter to remove small molecules and proteins from the blood. An important part of this filtration is the existence of tiny pores, called fenestrations, which extend through the entire thickness of the cell. Because these holes are only 50-200 nm in diameter, they have been impossible to study

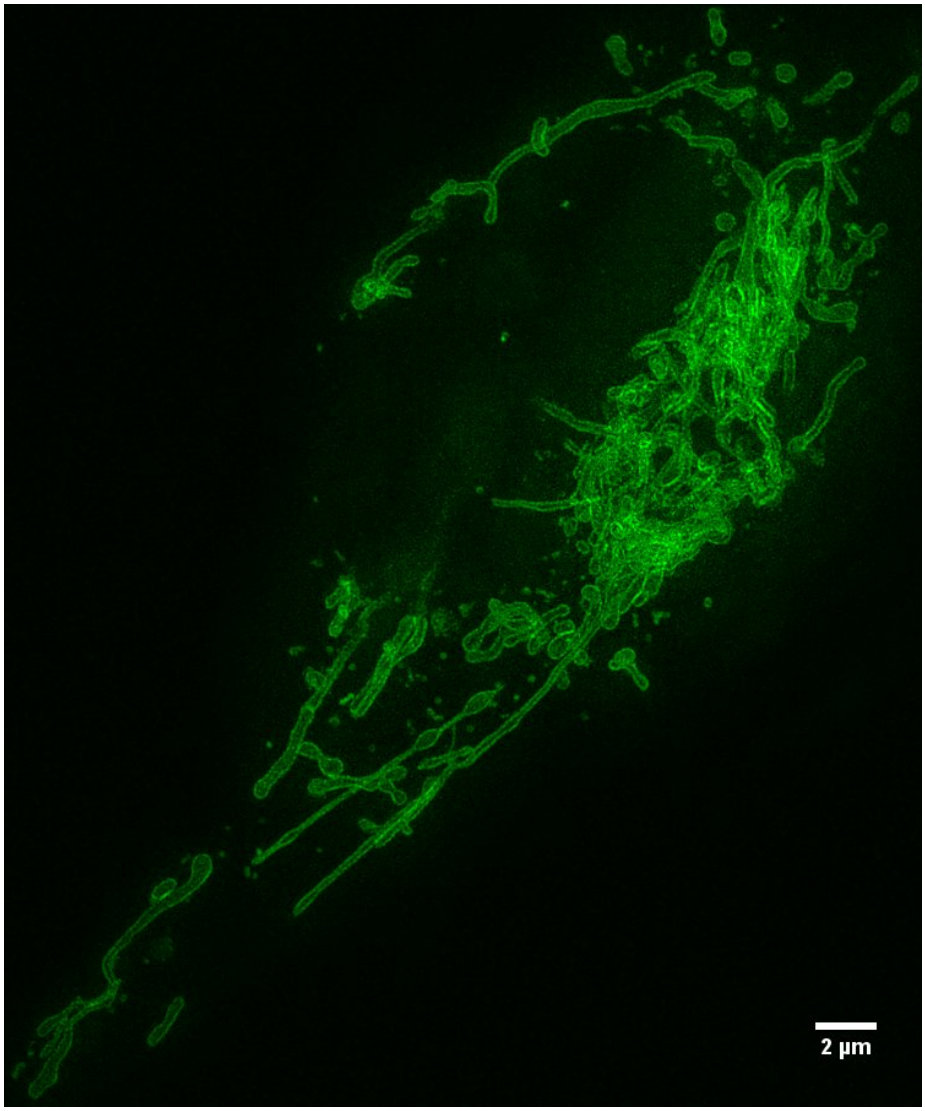

Figure 3.22: *3D-SIM image of MCC13 cell labeled with Gtom*, acquired immediately before the DV TL images shown in Figure 3.23. Projected 3 µm stack.

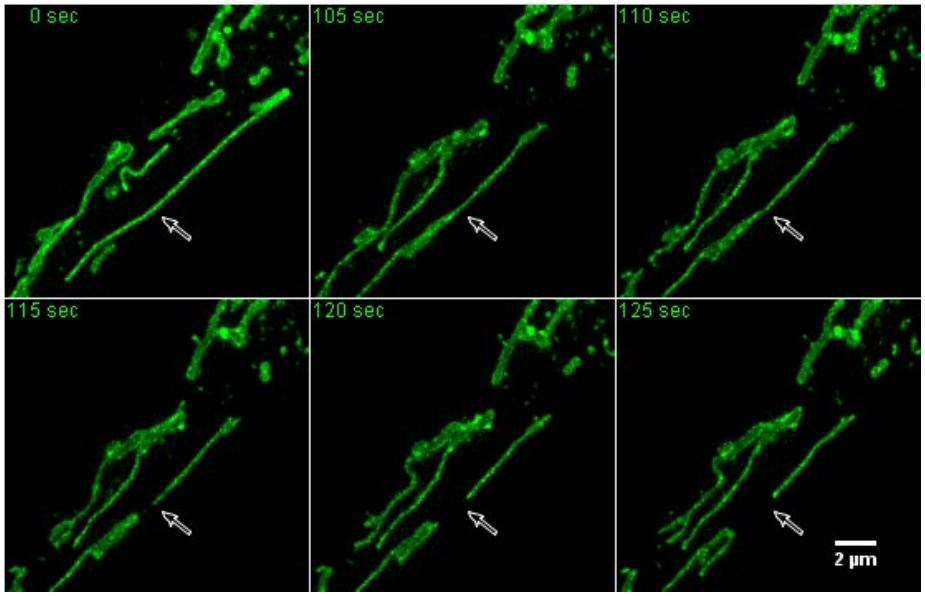

Figure 3.23: *DV time-lapse of previous SIM image.* The arrows indicate a splitting mitochondrion. Diffraction-limited DV proved to be a much better tool for monitoring mitochondrial dynamics. Combining SIM with DV gives access to both super-resolution and dynamics.

with conventional light microscopy, which is why VBRG was interested in using SIM[30].

Working with these cells is expensive both in terms of time and resources. Fenestrations disappear very quickly after the cells are isolated from a living animal (in these studies, a rat), so imaging traditionally has needed to be performed within a few hours after excision. However, rat LSECs (rLSECs) have recently been found to retain morphology and function after proper freezing, which has greatly increased the availability of rLSECs. They are still limited to some hours of (live) imaging, which makes them unsuitable for transfection experiments, but turned out to be good candidates for labeling with MitoTracker. Combining our research interests, (i.e. super-resolved imaging of mitochondria *plus* of LSEC membrane fenestrations), resulted in dual-staining experiments using MT and the plasma membrane stain CellMask. The results are presented below.

3.2.1 MitoTracker

To study the mitochondrial morphology and distribution in living rLSECs with 3D-SIM, the cells were stained with MTG as described in Chapter 2. Despite very different morphology and function of these (liver) cells compared to the skin cells studied in previous section, the structure (of the intermembrane space) revealed by MT appears to be very similar, as seen e.g. in Figure 3.24 which shows the projected 3D-SIM image of the mitochondria of an (entire) living rLSEC, and Figure 3.25 for a line profile-comparison between a single slice SIM image (*left*) versus the corresponding WF image (*right*) of the same plane. As for the mitochondria studied in the previous section, their internal structure is diffraction-limited and SIM can provide some additional detail about this compared to conventional microscopy.

Figure 3.26 provides a line profile also for mitochondria stained with MTdr (ex. λ= 642 nm), and the two colors of MT seem to label the same structures, without the worse resolution provided by MTdr (because of the longer emitted λ) obscuring structures substantially.

MitoTracker Overstaining

An accidental overstaining with MTG led to the discovery of some previously unrecognized structures in rLSECs, which were quickly named tubes; one of these is pointed out by the arrow in Figure 3.27. Movie 6 on the CD shows a rotation of this structure in 3D, so we can see that it actually is a tube.

If we compare the cell overstained with MTG with the optimally stained (healthy cell) in Figure 3.24, the morphological difference between the mitochondria of the two cells is striking: what is left of the elongated structures seen during this thesis on live cell imaging are small spheres (or circles in 2D), probably similar to how they appear fixed in electron microscopy.

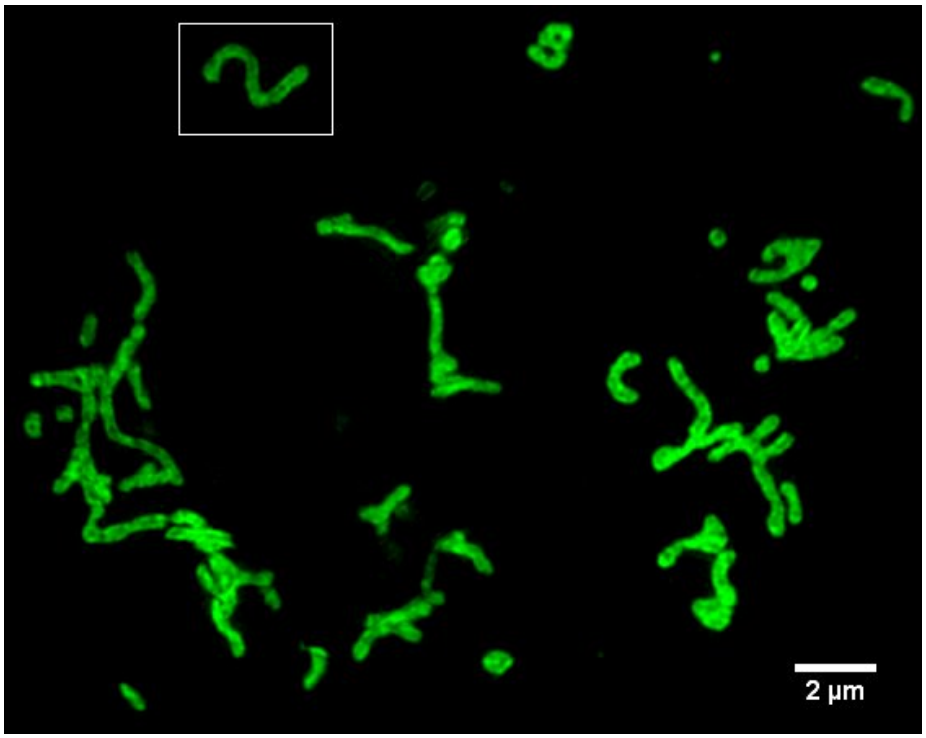

Figure 3.24: *Live rLSEC stained with MTG (ex. λ= 488 nm).* The square indicates a mitochondrion investigated further in the next figure. Projected 3D-SIM image.

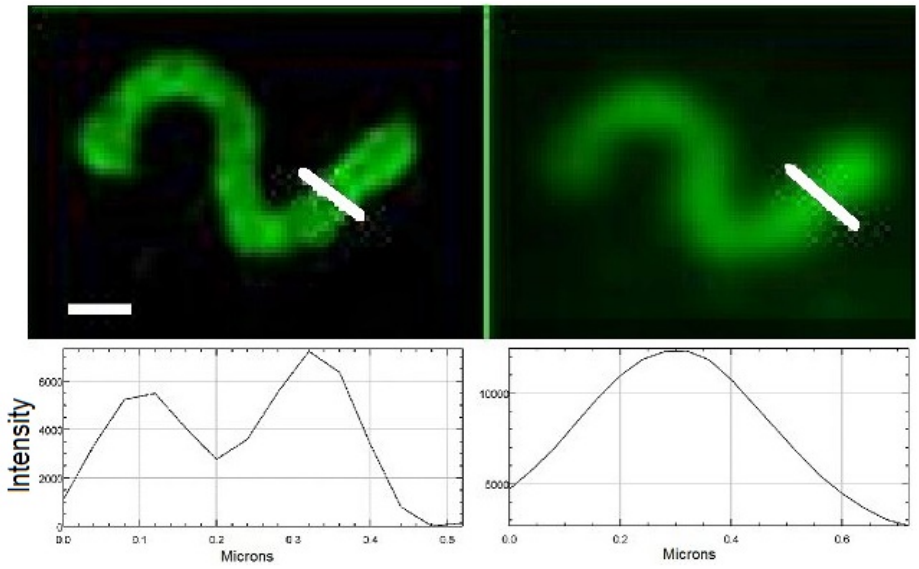

Figure 3.25: *SIM-WF comparison of mitochondria in rLSEC stained with MTG (ex. λ= 488 nm).* The intensities along the lines drawn in the upper images are plotted in the graphs below. The SIM image shows two distinct features along the line where the DV image can only resolve one. Scale bar 0.5 µm.

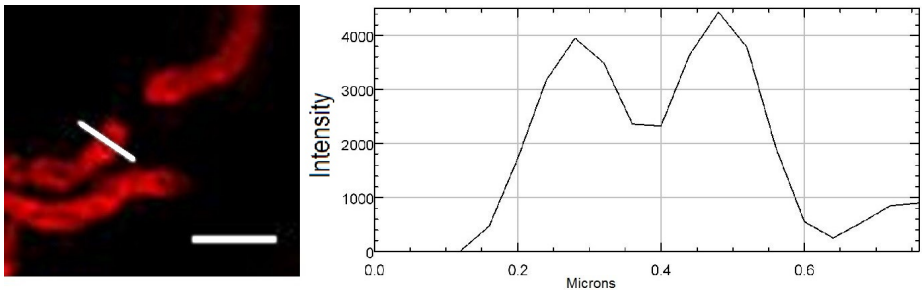

Figure 3.26: *Mitochondria stained using MTdr (ex. λ= 642 nm) reveals similar structures as when stained using MTG.* Single slice SIM image with the intensities along the indicated line plotted to the right. Scale bar 1 µm.

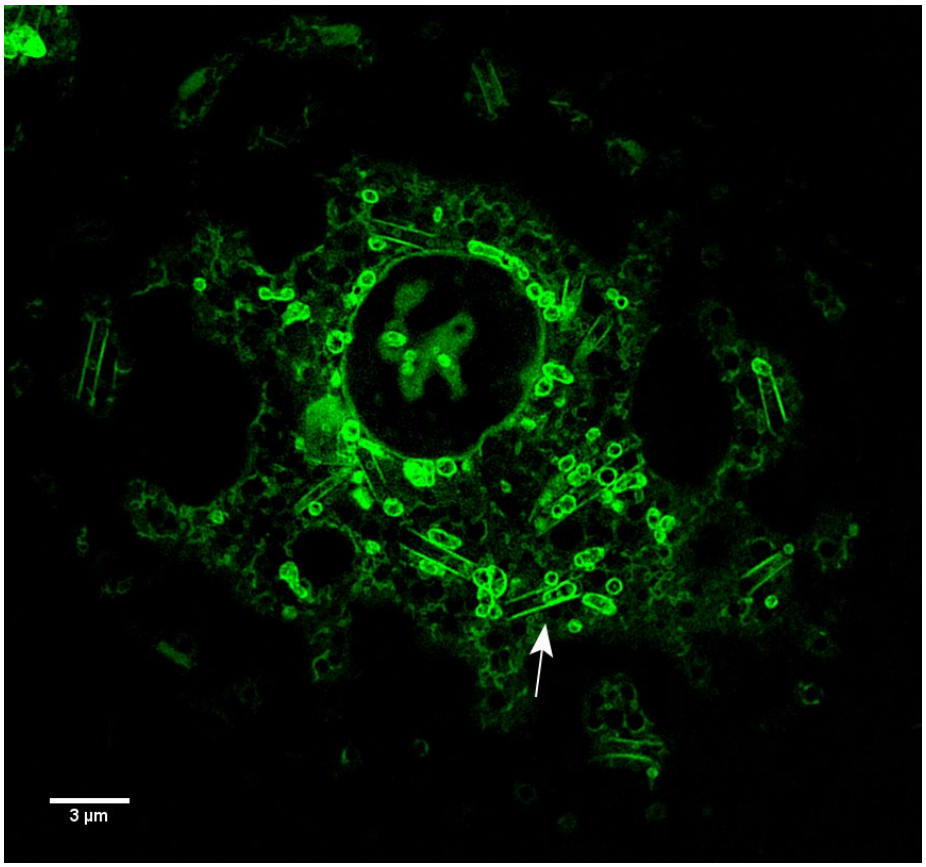

Figure 3.27: *Overstaining of rLSEC with MTG revealed new subcellular structures.* The arrow indicates something looking like a mitochondrion in a tube. Single slice SIM image.

Time-Lapse

Optimization for time-lapse was also done on rLSECs, with results very similar to what described in the previous section, sphering included. It was first discovered using MTG (ex. λ= 488 nm), and MTdr was tried to test if using a longer wavelength for imaging would cause less morphological artifacts. This was because green light has been shown to be far more damaging to cells than red (longer λ) light[6].

The results showed that MTdr caused *at least* as much artifacts as MTG. An example of this is shown in Figure 3.28, where mitochondria becomes wider and shorter during the repeated light exposure of only six 3D-SIM images acquired with low intensities (1%T for 4 ms) and staining done at moderate concentrations (75 nM for 30 min).

Remembering the previous discussions about photobleaching, ROS and cellular damage (sections 1.3.2 and 3.1.6), it is interesting to note that the mitochondria become darker when the widening is strongest, as if whatever supported the elongated structure of mitochondria was mutually affected by the excited fluorophores, resulting in bleaching of the fluorophores and also 'collapse' of the mitochondria towards a more spherical shape (requiring less surface energy). In the top row of Figure 3.28, little change is noticeable, while in the second row all three mitochondria become darker and wider, so the bleaching and morphological artifacts seem to happen *at the same time*.

3.2.2 CellMask

To see diffraction-limited fenestrations, rLSECs were incubated with the membrane stains CellMask Orange (CMO) (ex. λ= 568 nm) and CellMask Deep Red (CMdr) (ex. λ= 642 nm). Only the CMdr showed satisfying results live, meaning resolving the diffraction-limited fenestrations, preferably located in sieve plates. The negative results with CMO was possibly caused by using old dye, but other experiments showed that the CMO was still providing satisfactory staining on *fixed* cells, as shown in Figure 3.29**A**. Figure 3.29**B** shows the same batch of CMO staining *living* rLSECs. LSECs are 'dirt removers' important in the blood clearance function, so a likely explanation for why this experiment failed to work *live* is that the dye was quickly endocytosed ('taken within') or degraded by the cells. A different staining protocol with shorter incubation time and/or a fresher dye might have proven better for this particular live-cell membrane study.

CellMask Deep Red (ex. λ= 642 nm) showed better results live. As illustrated in Figure 3.30**A**, the membrane fenestrations are stained, intact and resolvable with SIM, but not with wide-field (WF), **B**. From the WF image one can tell from the darker regions where the sieve plates might be, but not resolve the fenestrations, as is the case for SIM.

There are, however, fenestrations unresolvable also for SIM. According to [40], 'fenestrations are approximately 50–150 nm in diameter and most are aggregated into groups of 10–100, so-called liver sieve plates'. Since the resolution

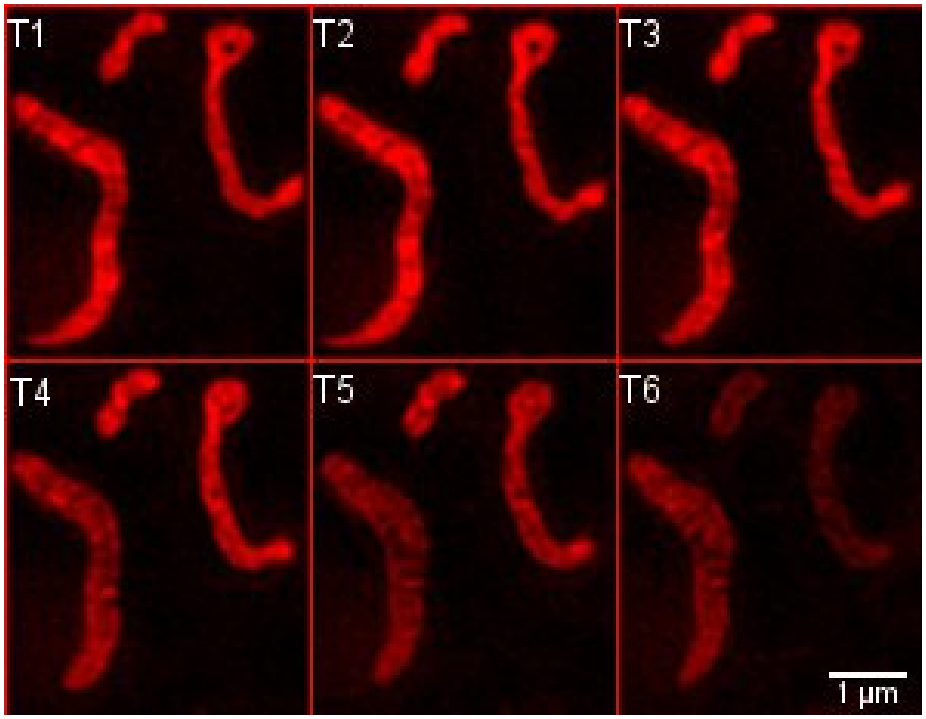

Figure 3.28: *Time-lapse of mitochondria within a living rLSEC stained with MTdr.* Even at low concentrations of MTdr (75 nM), long wavelength excitation light (642 nm) and low light exposure (1%T, 4 ms), the mitochondria expand and shorten (sphere-up) during imaging, at the same time as bleaching occurs. The time-points are acquired every 1 minute.

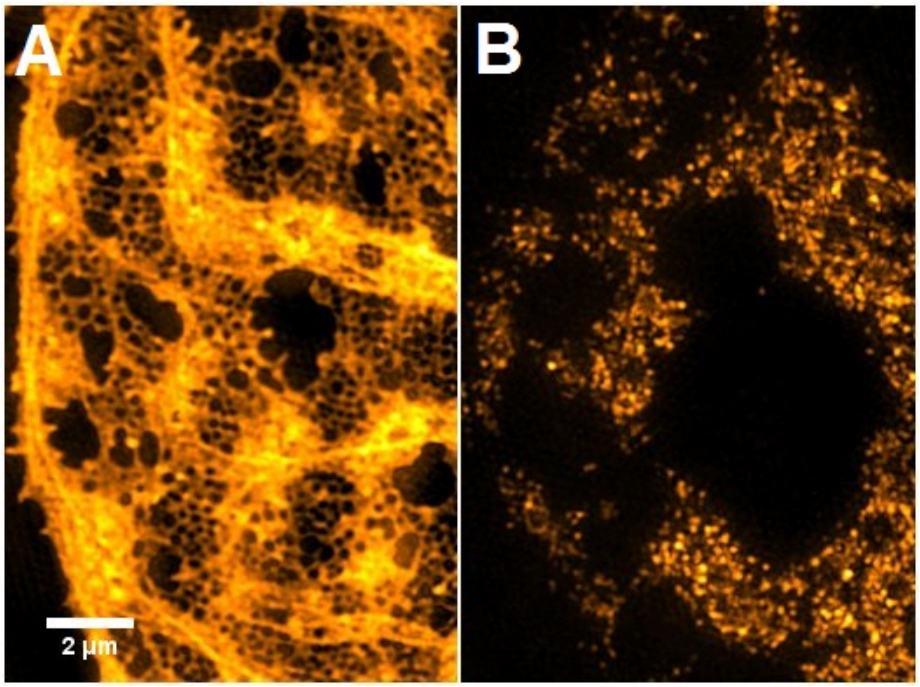

Figure 3.29: *rLSECs stained with CMO* (ex. λ= 568 nm). **A**: Fixed in PFA before staining. **B**: Staining living cells. Projected 3D-SIM images.

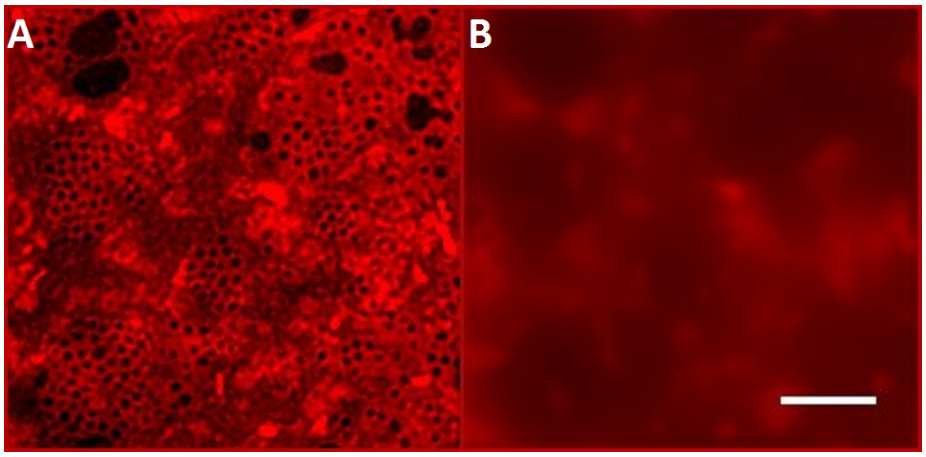

Figure 3.30: Live rLSEC stained with CellMask Deep Red (ex. λ= 642 nm). **A** Projected 3D-SIM image of a 1.5 µm stack, **B** Corresponding widefield image. Scale bar 2 µm

for this color channel only is 130 nm, there are probably many membrane holes unresolved also in the SIM image (**A**).

Figure 3.31 gives a magnified view of a small sieve plate with a line profile plotted to the right. The fenestrations actually seem to be 130-150 nm, as would be expected from the available resolution and previous liver studies.

3.2.3 MitoTracker and CellMask

The distribution of mitochondria within the cell membrane was revealed by dual-color experiments using MTG (ex. λ= 488 nm) and CMdr (ex. λ= 642 nm). A 3D visualization is given in movie 7. This illustrates the extreme flatness of

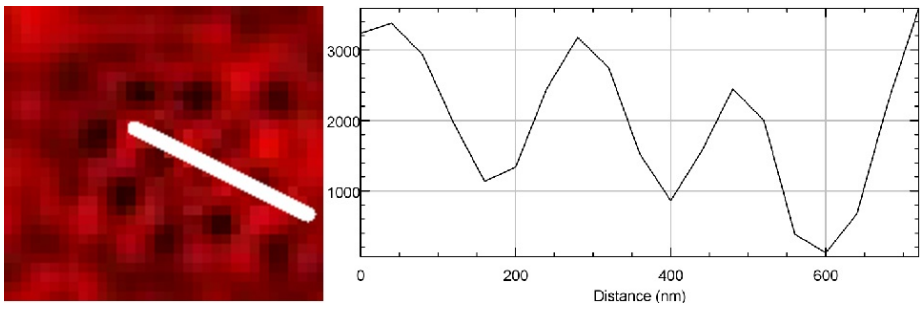

Figure 3.31: Projected 3D-SIM images (1.5 µm stack) of sieve plates in rLSEC stained with CellMask Deep Red (ex. λ= 642 nm)and (to the right) a plot of the indicated line profile.

rLSECs, which (together with the diffraction-limited fenestrations) make them desired objects for many SR experiments. Also a projected 3D-SIM image of the same combination of stains is shown in Figure 3.32. A second cell is partly visible in the upper right corner and is connected to the center cell by a band of membrane. The 3D visualization of Movie 8 reveals that this band is actually a *tube* bridging the cells.

3.2.4 Membrane Time-Lapse

The diffraction-limited fenestration *through* LSECs are thought to open and close during their usual blood-clearing work. This is, however, beyond both conventional and fixed studies to confirm, so it has remained just a theory. With the new *live*-cell *nano*scope this became possible to confirm.

After optimizing imaging parameters for time-lapse (TL) of CMdr, fenestrations were confirmed opening and closing, as shown in Figure 3.33. The arrows each indicate some fenestration opening and/or closing, but the dynamics are best observed by movie 9 (on repeat), which shows a 4 minute time-lapse (8 frames) of projected 3D-SIM images of a 1.5 µm stack. Some examples of fenestrations opening/closing are also here indicated by arrows.

Using high intensities (above T=1%) the membrane seemed to quickly become motionless. Combining 1% T with around 10 ms exposure time, the signal was also sufficient for SIM reconstruction. By extending the time between each 3D-SIM image to 30 seconds, fenestration dynamics became abundantly visible. However, closer analysis of the 3D-data revealed that the opening and closing does not occur in all planes at the same time, but rather seems to be a result of thin moving folds (as opposed to the entire membrane squeezing together).

The opening and closing of nano-holes in liver membrane was an interesting finding for Vascular Biology Research Group and they will continue this research as a separate study.

3.3 SIM Artifacts

SIM is a reconstruction method, and is hence prone to various artifacts. They are usually caused by low signal-noise-ratio (s/n), photobleaching or mismatched oil.

For example, Figure 3.34 shows two points from a time-lapse (TL) on rLSECs stained with CMdr. Image **A** is the first image in the TL, while image **B** is the second TL point (30 seconds later). Image **A** shows *irregularly* arranged fenestrations in sieve-plates (as seen in section 3.2) and seemingly the reconstruction has worked. Image **B** on the other hand, displays a *regularly repeating* pattern, which looks like a characteristic *honeycomb* pattern, a typical SIM artifact. The honeycomb artifact can look confusingly similar to real membrane fenestrations (as in Figure 3.34**A**), so caution has to be taken when analyzing the reconstructed data.

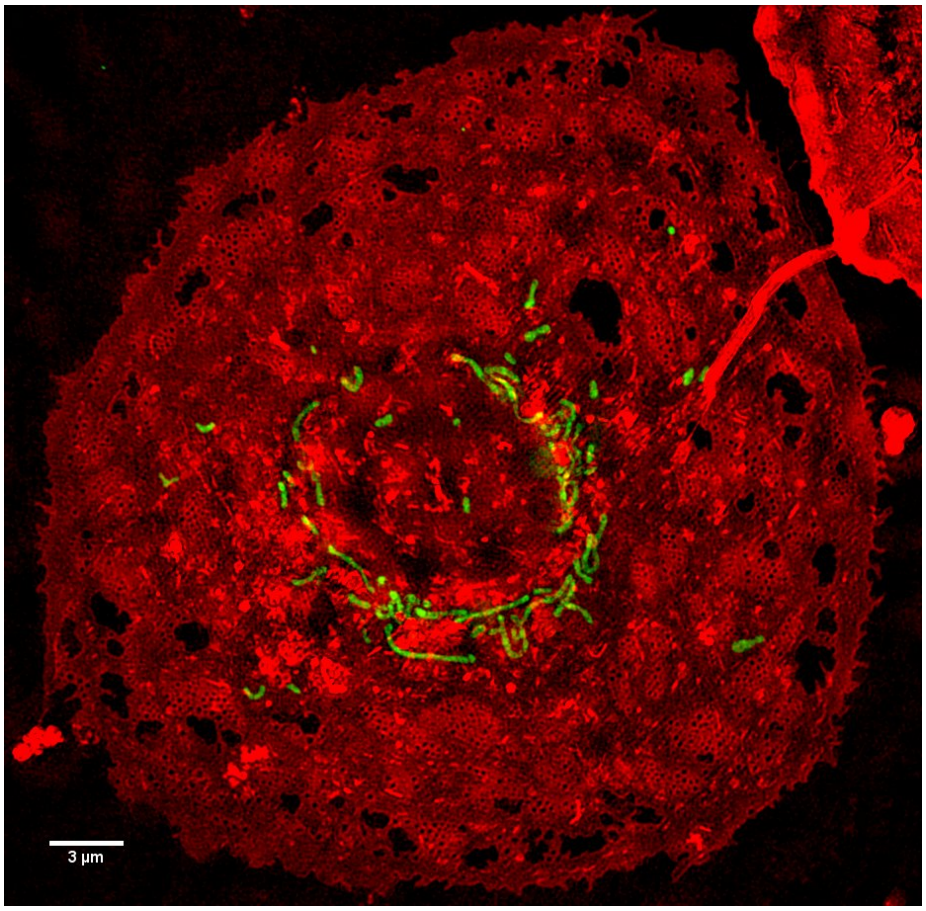

Figure 3.32: *Dual-color 3D-SIM image of rLSEC,* stained using MTG (ex. λ= 488 nm) in green and CMdr (ex. λ= 642 nm) in red. Projected image. Movie 8 shows (in 3D) that the dark red curve towards the upper right corner is actually a tube connecting the two cells.

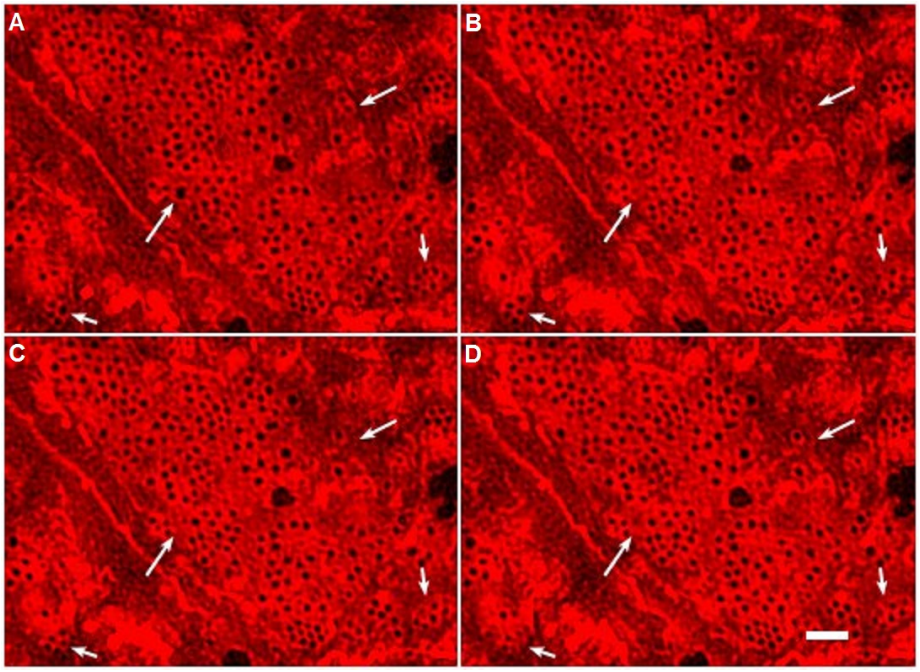

Figure 3.33: *Time-lapse of rLSECs showing fenestration dynamics.* 3D-SIM TL of rLSECs stained using CMdr (ex. λ= 642 nm) at four different time-points A, B, C and D (30 seconds between each). The arrows are indicating disappearing holes. Projected images. Scale bar 1 µm.

Figure 3.35 shows the honeycomb artifact on a much larger scale, where the artifact is much more obvious, and the cells (with mitochondria) visible in the wide-field image **B**, are not recognizable after reconstruction.

These cells are brightly labeled (also compared to the background), so the issue here is not s/n, but more likely *too much scattered light* blurring or warping the striped excitation pattern assumed by the reconstruction algorithm, causing errors.

Mismatch of the PSF *assumed* by the reconstruction algorithm, and the *actual* PSF of the imaging system causes artifacts typically seen as haloing or doubling. This results from *changes in the imaging system* due to variables like sample distance from coverslip, wavelength, temperature, immersion medium (of the cells) or coverslip thickness. This problem is addressed by changing the refractive index of the immersion oil on the microscope objective. Figure 3.36 shows a table illustrating how the optimal oil varies with the wavelength and sample position. From this, one can infer that multiple colors and large stacks severely increases the chances for reconstruction artifacts, but also that the effect is somewhat predictable and could be possible to adjust for in the reconstruction algorithm (in some hopefully near-future SIM software).

Another type of error is caused by *photobleaching*, which (as mentioned in 1.3.2) is permanent fading of the fluorophores. Since the reconstruction algorithm assumes that the sample does not change or move during the imaging process, the decreases in intensity during the acquisition of a 3D-SIM image (recall: 120 2D-images per 1 µm sample thickness) can cause errors. As a rule of thumb, the decrease in signal during the acquisition of a z-stack should be no more than 30%[42]. Photobleaching is best avoided by lowering the excitation intensities and choosing photostable fluorophores.

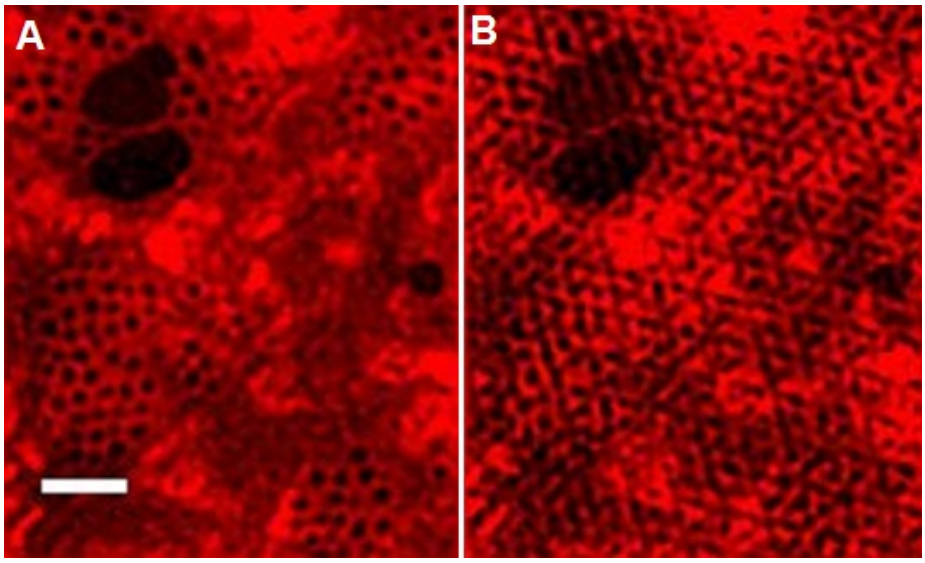

Figure 3.34: *Honeycomb artifacts from low signal-to-noise.* **A**: First time-point (TP) from SIM TL with irregularly arranged holes (and good reconstruction). **B**: Second TP of SIM TL, not good reconstruction recognized by the regularly repeating pattern. Projected 3D-SIM images of rLSEC stained with CMdr. Scale bar 1 µm.

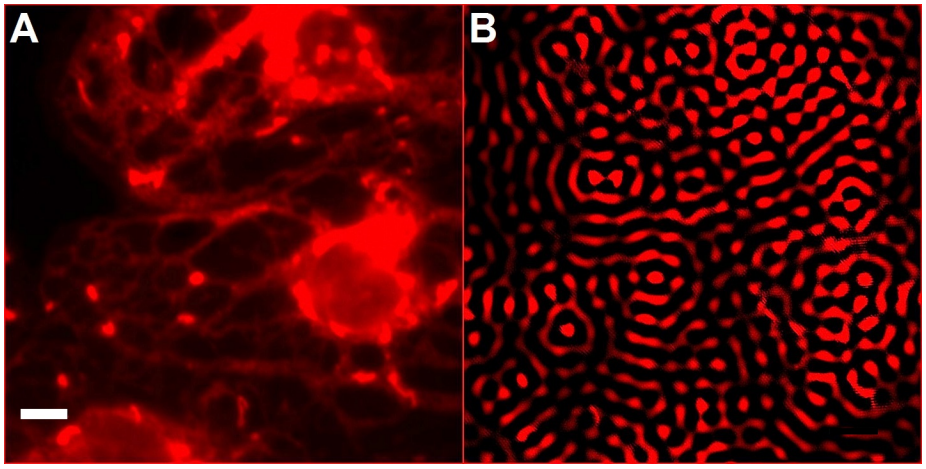

Figure 3.35: *Wide-field - SIM comparison (honeycomb artifacts).* **A**: Wide-field image, **B**: Poorly reconstructed SIM image. Over-staining causes reconstruction artifacts and makes structures visible in the wide-field image (**A**) unrecognizable in the SIM image (**B**). Projected images of rLSECs stained with 400 nM MTdr. Scale bar 4 µm.

Emitted Wavelength (nm)	Imaging at the coverslip	Imaging 5um above coverslip	Imaging 10um above coverslip
405	1.510	1.512	1.514
488	1.512	1.514	1.516
568	1.514	1.518	1.520
642	1.518	1.520	1.522

Figure 3.36: Table illustrating how the refractive index for the optimal oil varies for different wavelengths and sample positions.[43]

Chapter 4

Conclusions

We have seen that multicolor live cell imaging with 3D-SIM indeed is possible and that the extra resolution provided allows for studying dynamics otherwise hidden in absence of SR capabilities, like the opening and closing of fenestrations through the membrane of LSECs. The structure of mitochondria in up to three colors was accomplished, pushing the limits of fluorescent probes and the SIM system, which has a maximum resolution of 100 nm under suitable staining conditions.

Multicolor imaging comes with the cost of invasiveness and imaging time, but can also aid in the recognition of *staining artifacts*, like the reduced retention of MT in BM transduced cells. Both MTG and MTdr were shown to cause morphological artifacts when used for 3D-SIM time-lapse imaging of mitochondrial, typically sphering. This effect was reduced by optimization of imaging parameters towards lower concentrations of MT and less light exposure.

SIM can work with many conventional stains, but not necessarily with the same staining protocols as for conventional microscopy. SIM is a reconstruction method, and hence prone to artifacts. Successful mapping of SR information imposes stricter requirements on the sample, especially concerning s/n, but also bleaching or mismatched oil can cause reconstruction failure.

When preparing samples, one should aim for using fluorophores with favorable photophysical properties (bright, non-bleaching) and densely, specifically labeled structures. When imaging *live* samples, invasiveness is also a prime concern, so the type of probe and labeling density must be carefully chosen according to one's specific application.

Luckily, new labeling techniques have emerged, making the future look bright for fluorescence nanoscopy. For example, one such example from New England Biolabs is described as 'the SNAP- and CLIP-tag protein labeling systems enable the specific, covalent attachment of virtually any molecule to a protein of interest'[45]. It seems like the technology for specific labeling of living cells with almost any desired fluorophore is already on the market, ready for super-resolution applications (but notably from the tongue of vendors).

Time-lapse imaging was done with SIM and comparable experiments with

diffraction-limited deconvolution microscopy (DV). SIM required higher signal-to-noise ratios for successful imaging and was light intensive compared to DV. SIM caused quick bleaching (limiting the number of frames possible) and clear phototoxic effects, resulting in morphological artifacts. In comparison, time-lapse with DV enabled more time-points, a larger field of view and resulted in no apparent morphological artifacts.

While optical nanoscopy could still be a preferred option for imaging a small number of time-points of diffraction-limited structures, the extra photon cost still makes DV a better tool for studies not strictly requiring the higher resolution (like monitoring mitochondrial dynamics).

Challenges in live cell fluorescence nanoscopy to be dealt with in the future includes improving the SIM reconstruction algorithm so that lower light exposure is required, finding fluorescent probes with improved photophysical properties that gives specific, non-toxic labeling of a flexible range of structures, and coupling of SIM with other microscopy techniques, enabling biological studies on a flexible scale.

Chapter 5

List of Publications

POSTERS ICON CONFERENCE JUNE 2016

1. Multicolor structured illumination microscopy of mitochondria in living cells. Ida S. Opstad, Deanna L. Wolfson, Cristina I. Øie, Balpreet S. Ahluwalia

2. Nanoscale dynamics of liver sinusoidal endothelial cells. Deanna L. Wolfson, Cristina I. Øie, Ida S. Opstad, Balpreet S. Ahluwalia

3. Mapping sub-cellular nanostructures and functions in a living sinusoidal endothelial liver cell by 3D-structured illumination microscopy. Cristina I. Øie, Hong Mao1, Ida S. Opstad, Deanna Wolfson, Peter A. McCourt, Balpreet S. Ahluwalia

4. Live cell fluctuation based SR imaging using high-frequency, near-field illumination patterns enabled by planar waveguides. Robin Diekmann, Øystein I. Helle, Ida S. Opstad, Deanna L. Wolfson, Thomas R. Huser, Balpreet S. Ahluwalia, and Mark Schüttpelz

MANUSCRIPT-IN-PREPARATION

1. Multicolor structured illumination microscopy of mitochondria in living cells. Ida S. Opstad, Deanna L. Wolfson, Cristina I. Øie, Balpreet S. Ahluwalia

Chapter 6

Bibliography

[1] B.E.A Saleh & M.C. Teich, *Fundamentals of photonics*, 2nd edition, page 448. John Wiley & Sons, Inc., Hoboken, New Jersey, 2007.

[2] E. Abbe, 'Beiträge zur Theorie des Mikroskops und der mikroskopischen Wahrnehmung' in *Arch. Mikrosk.* Anat. 9 413–420, 1873.

[3] Catherine G. Galbraith, James A. Galbraith. 'Super-resolution microscopy at a glance' in *Journal of Cell Science* 124, 1607-1611, 2011. doi:10.1242/jcs.080085

[4] Aurélie Jost and Rainer Heintzmann. 'Superresolution Multidimensional Imaging with Structured Illumination Microscopy' in *Annual Review of Materials Research* Vol. 43: 261-282, 2013. doi:10.1146/annurev-matsci-071312-121648

[5] Lothar Schermelleh, Rainer Heintzmann, and Heinrich Leonhardt. 'A guide to super-resolution fluorescence microscopy' in *The Journal of Cell Biology*, vol. 190 no. 2 165-175, 2010. doi:10.1083/jcb.201002018

[6] Sina Wäldchen, Julian Lehmann, Teresa Klein, Sebastian van de Linde & Markus Sauer. 'Light-induced cell damage in livecell super-resolution microscopy' in Scientific Reports, 2015. doi: 10.1038/srep15348

[7] Thermo Fisher Scientific, article on 'Fluorescent Probes'. https://www.thermofisher.com/no/en/home/life-science/protein-biology/protein-biology-learning-center/protein-biology-resource-library/pierce-protein-methods/fluorescent-probes.html, accessed on 2015-10-16.

[8] Nikon MicroscopyU, article on 'Phototoxicity in Microscopy Literature References'. https://www.microscopyu.com/references/phototoxicity.html, accessed on 2015-10-16.

[9] Daniel Evanko, article on 'Is phototoxicity compromising experimental results?' in *Methagore*, a blog from *Nature Methods*, http://blogs.nature.com/methagora/2013/11/is-phototoxicity-compromising-experimental-results.html, accessed on 2015-10-16.

[10] Article 'Beyond the diffraction limit' in *Nature Photonics*, http://www.nature.com/nphoton/journal/v3/n7/full/nphoton.2009.100.html, accessed on 2015-10-16.

[11] Nikon MicroscopyU, article on 'The Diffraction Barrier in Optical Microscopy', http://www.microscopyu.com/articles/superresolution/diffractionbarrier.html, accessed on 2015-10-16.

[12] Nikon MicroscopyU, article on 'Maintaining Live Cells on the Microscope Stage'. http://www.microscopyu.com/articles/livecellimaging/livecellmaintenance.html, accessed on 2016-04-16.

[13] Alberts B, Johnson A, Lewis J, et al. 'Looking at the Structure of Cells in the Microscope' in *Molecular Biology of the Cell. 4th edition*, New York: Garland Science, 2002. http://www.ncbi.nlm.nih.gov/books/NBK26880/

[14] Mats G.L. Gustafsson, Lin Shao, Peter M. Carlton, C. J. Rachel Wang, Inna N. Golubovskaya, W. Zacheus Cande, David A. Agard, John W. Sedat, 'Three-Dimensional Resolution Doubling in Wide-Field Fluorescence Microscopy by Structured Illumination', in *Biophysical Journal*, Volume 94, Issue 12, 15 June 2008, Pages 4957-4970, ISSN 0006-3495. doi:http://dx.doi.org/10.1529/biophysj.107.120345

[15] Stefan Jakobs. 'High resolution imaging of live mitochondria' in *Biochimica et Biophysica Acta (BBA) - Molecular Cell Research*, Volume 1763, Issues 5–6, May–June 2006, Pages 561-575, ISSN 0167-4889. doi:http://dx.doi.org/10.1016/j.bbamcr.2006.04.004

[16] Shim, S.-H., Xia, C., Zhong, G., Babcock, H. P., Vaughan, J. C., Huang, B., ... Zhuang, X. 'Super-resolution fluorescence imaging of organelles in live cells with photoswitchable membrane probes' in *Proceedings of the National Academy of Sciences of the United States of America*, 109(35), 13978–13983, 2012. doi::://doi.org/10.1073/pnas.1201882109

[17] Hoebe, R. A. Van Oven, C. H. Gadella, T. W. J. Dhonukshe, P. B. Van Noorden, C. J. F. Manders, E. M. M. 'Controlled light-exposure microscopy reduces photobleaching and phototoxicity in fluorescence live-cell imaging' in *Nat Biotech*, 2007.

[18] Heidi M. McBride, Margaret Neuspiel, Sylwia Wasiak. 'Mitochondria: More Than Just a Powerhouse' in *Current Biology*, Volume 16, Issue 14, 25 July 2006, Pages R551-R560, ISSN 0960-9822. doi:http://dx.doi.org/10.1016/j.cub.2006.06.054

[19] Nightsea, article on 'Physics of fluorescence – the Jablonski diagram'. http://www.nightsea.com/articles/jablonski-diagram-for-fluorescence/, accessed on 2016-05-07.

[20] Retrieved from http://www.nightsea.com/articles/jablonski-diagram-for-fluorescence/, 2016-05-07. Modified.

[21] Retrieved from https://en.wikipedia.org/wiki/Stokes_shift#/media/File:Stokes_shift-_Rh6G.png, 2015-10-20. Modified.

[22] Retrieved from www.glogster.com/davidzhang619/cell-organelles/g-6lsbpkf9dmb3d0gt4u5dma0, 2016-05-08. Modified.

[23] Zhe Liu, Luke D. Lavis, Eric Betzig. 'Imaging Live-Cell Dynamics and Structure at the Single-Molecule Level', in *Molecular Cell*, Volume 58, Issue 4, 21 May 2015, Pages 644-659, ISSN 1097-2765. doi:http://dx.doi.org/10.1016/j.molcel.2015.02.033

[24] B.G. Kopek, G. Shtengel, C.S. Xu, D.A. Clayton, H.F. Hess. 'Correlative 3D superresolution fluorescence and electron microscopy reveal the relationship of mitochondrial nucleoids to membranes', in *Proc. Natl. Acad. Sci.* USA, 109 (2012), pp. 6136–6141.

[25] Retrieved from https://en.wikipedia.org/wiki/Moir%C3%A9_pattern#/media/File:Moir%C3%A9_pattern.svg

[26] Ulrike Schnell, Freark Dijk, Klaas A Sjollema, Ben N G Giepmans. 'Immunolabeling artifacts and the need for live-cell imaging' in *Nature Methods* 9, 152–158 (2012). doi:10.1038/nmeth.1855

[27] Maksim V. Sednev, Vladimir N. Belov, Stefan W. Hell. 'Fluorescent dyes with large Stokes shifts for super-resolution optical microscopy of biological objects: a review' in *Methods and Applications in Fluorescence*, volume 3, number 4, 2015. http://stacks.iop.org/2050-6120/3/i=4/a=042004

[28] Michael Reth. 'Matching cellular dimensions with molecular sizes' in *Nature Immunology* 14, 765–767 (2013). doi:10.1038/ni.2621

[29] Michael Ratz, Ilaria Testa, Stefan W. Hell & Stefan Jakobs. 'CRISPR/Cas9-mediated endogenous protein tagging for RESOLFT super-resolution microscopy of living human cells' in *Scientific Reports* 5, 9592, 2015. doi:10.1038/srep09592

[30] Viola Mönkemöller, Cristina Øie, Wolfgang Hübner, Thomas Huser & Peter McCourt. 'Multimodal super-resolution optical microscopy visualizes the close connection between membrane and the cytoskeleton in liver sinusoidal endothelial cell fenestrations' in *Scientific Reports*, 2015. doi:10.1038/srep16279

[31] Alessandra Carattoli. 'Plasmids and the spread of resistance' in *International Journal of Medical Microbiology*, Volume 303, Issues 6–7, August 2013, Pages 298-304, ISSN 1438-4221, http://dx.doi.org/10.1016/j.ijmm.2013.02.001

[32] Mark A. Hink, Remko A. Griep, Jan Willem Borst, Arie van Hoek, Michel H. M. Eppink, Arjen Schots, and Antonie J. W. G. Visser. 'Structural Dynamics of Green Fluorescent Protein Alone and Fused with a Single Chain Fv Protein' in *J. Biol. Chem*, 2000. doi:10.1074/jbc.M001348200

[33] Eva Bianconi, Allison Piovesan, Federica Facchin, Alina Beraudi, Raffaella Casadei, Flavia Frabetti, Lorenza Vitale, Maria Chiara Pelleri, Simone Tassani, Francesco Piva, Soledad Perez-Amodio, Pierluigi Strippoli, Silvia Canaider. 'An estimation of the number of cells in the human body' in *Annals of Human Biology* Vol. 40, Iss. 6, 2013. doi:10.3109/03014460.2013.807878

[34] Griffiths AJF, Miller JH, Suzuki DT, et al. *An Introduction to Genetic Analysis*. 7th edition. New York: W. H. Freeman; 2000. Transduction. Available from: http://www.ncbi.nlm.nih.gov/books/NBK21760/

[35] J S Collins, T H Goldsmith. 'Spectral properties of fluorescence induced by glutaraldehyde fixation' in *Journal of Histochemistry and Cytochemistry*, 04/1981; 29(3):411-4. doi: 10.1177/29.3.6787116

[36] Thermo Fisher Scientific. Description of 'CellLight Mitochondria-RFP, BacMam 2.0'. url-https://www.thermofisher.com/order/catalog/product/C10505

[37] Genetics Home Reference. http://ghr.nlm.nih.gov/gene/PDHA1

[38] Stefan Jakobs, Christian A Wurm. 'Super-resolution microscopy of mitochondria' in *Current Opinion in Chemical Biology*, 2014. doi:10.1016/j.cbpa.2014.03.019

[39] Stefan Jakobs. 'High resolution imaging of live mitochondria', *Biochimica et Biophysica Acta (BBA) - Molecular Cell Research*, Volume 1763, Issues 5–6, May–June 2006, Pages 561-575, ISSN 0167-4889, http://dx.doi.org/10.1016/j.bbamcr.2006.04.004.

[40] Svistounov D, Warren A, McNerney GP, Owen DM, Zencak D, Zykova SN, et al. (2012) 'The Relationship between Fenestrations, Sieve Plates and Rafts in Liver Sinusoidal Endothelial Cells' in *PLoS ONE* 7(9): e46134. doi:10.1371/journal.pone.0046134

[41] Alberts B, Johnson A, Lewis J, et al. 'Electron-Transport Chains and Their Proton Pumps', *Molecular Biology of the Cell*, 4th edition. New York: Garland Science, 2002. Available from http://www.ncbi.nlm.nih.gov/books/NBK26904/

[42] Patrina Pellett (GE Healthcare). Webinar on 'Super-Resolution Imaging', May 6th 2015. Available from http://www.gelifesciences.com/gehcls_images/GELS/Pdf\%20documents/2015-05-06-Pellett-Bitesizebio-Seminar.pdf

[43] Retrieved from Patrina Pellett (GE Healthcare). Webinar on 'Super-Resolution Imaging', May 6th 2015. Modified. Available from http://www.gelifesciences.com/gehcls_images/GELS/Pdf\%20documents/2015-05-06-Pellett-Bitesizebio-Seminar.pdf

[44] New England Biolabs homepage, article on 'Protein Labeling (SNAP/CLIP)'. https://www.neb.com/applications/protein-analysis-and-tools/protein-labeling/protein-labeling-snap-clip

[45] Arnaud Gautier, Alexandre Juillerat, Christian Heinis, Ivan Reis Corrêa Jr., Maik Kindermann, Florent Beaufils, Kai Johnsson. 'An Engineered Protein Tag for Multiprotein Labeling in Living Cells' in *Chemistry & Biology*, Volume 15, Issue 2, 22 February 2008, Pages 128-136, ISSN 1074-5521. http://dx.doi.org/10.1016/j.chembiol.2008.01.007

[46] David A. Boas, Constantinos Pitris, Nimmi Ramanujam. *Handbook of Biomedical Optics*, page 63. CRC Press, 2016.

[47] Andrey V. Kuznetsov, Martin Hermann, Valdur Saks, Paul Hengster, Raimund Margreiter. 'The cell-type specificity of mitochondrial dynamics' in *The International Journal of Biochemistry & Cell Biology*, Volume 41, Issue 10, October 2009, Pages 1928-1939, ISSN 1357-2725. http://dx.doi.org/10.1016/j.biocel.2009.03.007

[48] Larry Simpson, Frank Kretzer. 'The mitochondrion in dividing Leishmania tarentolae cells is symmetric and circular and becomes a single asymmetric tubule in non-dividing cells due to division of the kinetoplast portion' in *Molecular and Biochemical Parasitology*, Volume 87, Issue 1, July 1997, Pages 71-78, ISSN 0166-6851. http://dx.doi.org/10.1016/S0166-6851(97)00044-3.

Appendices

Appendix A

CD Content

Movies

1. Projected 3D-SIM time-lapse of mitochondria in MCC13 cell labeled using Gtom. Left side illustrates the quick bleaching of FPs using SIM, while the right side shows the same time-lapse bleach corrected, enabling studies of super-resolved mitochondrial dynamics. 10 seconds between each frame.
2. Large field of view DV time-lapse (8 µm z-projection) of mitochondria in MCC13 cells labeled using MTdr. 30 seconds between each frame, and with a total time of 30 minutes.
3. Large field of view DV time-lapse (7 µm z-projection) of mitochondria in MCC13 cells labeled using BM. 30 seconds between each frame, and with a total time of 20 minutes.
4. Large field of view DV time-lapse (7 µm z-projection) of mitochondria in MCC13 cells labeled using Gtom. 30 seconds between each frame, and with a total time of 30 minutes.
5. DV time-lapse (5 µm z-projection) of mitochondria in MCC13 cell labeled using Gtom. 5 seconds between each frame, and with a total time of 30 seconds.
6. 3D-SIM movie of tube in rLSEC overstained using MTG.
7. 3D of rLSEC stained using CMdr and MTG showing rLSEC morphology and distribution of mitochondria.
8. 3D-SIM movie of tube between rLSECs dually stained using MTdr and MTG.
9. Projected 3D-SIM time-lapse showing dynamics of rLSEC membrane stained using CMdr with arrows indicating examples of fenestrations opening/closing.

Appendix B

Microscope/Software

Microscope

Images were acquired with DeltaVision OMX V4 Blaze imaging system.
Reconstruction software: SoftWoRx 3D-SIM reconstruction software.
Objective: 60X oil immersion with 1.42 N.A.
Available lasers (100 mW): 405 nm, 488 nm, 568 nm, 642 nm.

Image Processing

Image processing was done using Fiji.
3D-movies were made using Volocity.